UNIVERSIDADE DA CORUÑA
Facultade de Ciencias

Chemistry Degree/ Grao en Química/ Grado en Química

Memoria do Traballo de Fin de Grao

Towards the preparation of chiral plasmonic nanostars

Cara á preparación de nanoestrelas plasmónicas quirais

Hacia la preparación de nanoestrellas plasmónicas quirales

Lucía del Carmen Sanz Figueroa

Curso: 2022 – 2023

Convocatoria: Xuño

Directores: Jesús Mosquera Mosquera
Alejandro Criado Fernández

Agradecimientos

A todo el grupo NanoSelf, por la atención, orientación y motivación. Por todos los consejos profesionales y personales. Y por hacerme ir al laboratorio con ganas todos los días.

A mis amigos, los que estaban y siguen estando, y a aquellos que he conocido en esta etapa. Por acompañarme en este camino y hacerlo más liviano. Agradezco mucho vuestra amistad y el tiempo que habéis dedicado a escucharme y ayudarme en momentos clave.

Y sobre todo a mi familia, en especial a mi madre, mi abuela y mi hermano, por todo el amor que me habéis dado siempre, por vuestra comprensión y paciencia, incluso cuando las cosas no salían bien. Por ser el punto al que sé que siempre podré acudir y un pilar fundamental en mi crecimiento personal, y por vuestra dedicación y buenos valores enseñados.

Por último, al motor que me ha impulsado hasta aquí, mi padre, quien me enseñó el valor de la educación y me brindó el apoyo incondicional que necesitaba para completar mi carrera. Cada obstáculo que superé, lo hice con su memoria en mi corazón, recordando sus palabras y su confianza en mí. Al final sí que tenía razón y todo acabaría saliendo bien.

ABBREVIATIONS AND ACRONYMS

Au NPs: Gold Nanoparticles

Au NRs: Gold Nanorods

Au NSs: Gold nanospheres

AA: Ascorbic Acid

NMs: Nanomaterials

CTAB: Cetyltrimethylammonium bromide

CTAC: Cetyltrimethylammonium chloride

NPs: Nanoparticles

TEM: Transmission Electron Microscopy

UV-Vis: Ultraviolet-visible

TEOS: Tetraethoxysilane

APTES: (3-Aminopropyl)iethoxysilane

LSPR: Localized Surface Plasmon Resonance

SPR: Surface Plasmon Resonance

SPB: Longitudinal Surface Plasmon Band

SERS: Surface Enhanced Raman Spectroscopy

MSSNs: Mesoporous Silica Nanoparticles

AuMSSs: Gold-core silica shell nanoparticles

nm: Nanometers

NIR: Near-Infrared

m/z: Mass-to-charge ratio

TLC: Thin-Layer Chromatography

δ: chemical shift

λ: Wavelenght

BINOL: [1,1'-binaphthalene]-2,2'-diol

ESI-MS: Electrospray Ionization Mass Spectrometry

m: multiplet

s: singlet

d: doublet

Contents

Abstract

Plasmonic nanoparticles (NPs) exhibit extraordinary optical properties that stem from their ability to sustain localized surface plasmon resonances. These resonances can be finely tuned by carefully controlling the morphology of the particles, allowing for optimization across a diverse range of applications. Recently, preparing chiral morphologies for these NPs has received considerable attention because it may provide important advantages in fields such as biomedicine. Thus, this undergraduate project focuses on the preparation of a novel type of plasmonic chiral NPs, i.e., chiral gold nanostars.

This TFG has been divided into three parts. The first part focuses on synthesizing and characterizing achiral gold nanostars, utilizing UV-Vis spectroscopy and TEM to analyze their morphological and optical properties. The second part involved attempting to introduce chirality into the gold nanostars by replacing the previous surfactant with a chiral one. Unfortunately, the desired results were not achieved. Consequently, in the third part, a new chiral surfactant was synthesized, although due to the project's limited duration, the verification of its effect on achieving chirality in the gold nanostars could not be completed. The chiral surfactant was characterized using ^{1}H-NMR, ^{13}C-NMR spectroscopy, and MS spectrometry.

Key words: nanomaterials, gold nanoparticles, gold nanostars, chirality, surface plasmon resonance, surfactant.

Resumo

As nanopartículas plasmónicas (NPs) presentan propiedades ópticas extraordinarias que se derivan da súa capacidade para manter as resonancias plasmónicas de superficie localizadas. Estas resonancias pódense afinar controlando coidadosamente a morfoloxía das partículas, permitindo a optimización nunha ampla gama de aplicacións. Recentemente, a preparación de morfoloxías quirais para estes NP recibiu unha atención considerable porque pode proporcionar importantes vantaxes en campos como a biomedicina. Polo tanto, este proxecto de pregrado céntrase na preparación dun novo tipo de NPs quirais plasmónicas, as nanoestrelas quirais de ouro.

Este TFG dividiuse en tres partes. A primeira parte céntrase na síntese e caracterización de nanoestrelas aquirales de ouro, utilizando espectroscopia UV-Vis e TEM para analizar as súas propiedades morfolóxicas e ópticas. A segunda parte consistiu en intentar introducir quiralidade nas nanoestrelas de ouro substituíndo o tensioactivo anterior por outro quiral. Desafortunadamente, non se conseguiron os resultados desexados. En consecuencia, na terceira parte, sintetizouse un novo surfactante quiral, aínda que debido á limitada duración do proxecto non se puido completar a verificación do seu efecto na consecución da quiralidade nas nanoestrelas de ouro. O surfactante quiral caracterizouse por espectroscopia ^{1}H-RMN, ^{13}C-RMN e espectrometría MS.

Palabras chave: nanomateriais, nanopartículas de ouro, nanoestrelas de ouro, quiralidade, resonancia plasmática superficial, surfactante.

Resumen

Las nanopartículas plasmónicas (NPs) exhiben propiedades ópticas extraordinarias que se derivan de su capacidad para sostener resonancias de plasmones superficiales localizadas. Estas resonancias se pueden ajustar con precisión controlando cuidadosamente la morfología de las partículas, lo que permite la optimización en una amplia gama de aplicaciones. Recientemente, la preparación de morfologías quirales para estas NPs ha recibido una atención considerable porque puede proporcionar importantes ventajas en campos como la biomedicina. Por lo tanto, este proyecto de pregrado se centra en la preparación de un nuevo tipo de NP quirales plasmónicas, las nanoestrellas de oro quirales.

Este TFG se ha dividido en tres partes. La primera parte se centra en sintetizar y caracterizar nanoestrellas de oro aquirales, utilizando espectroscopia UV-Vis y TEM para analizar sus propiedades morfológicas y ópticas. La segunda parte consistió en intentar introducir quiralidad en las nanoestrellas de oro reemplazando el surfactante anterior por uno quiral. Desafortunadamente, no se lograron los resultados deseados. En consecuencia, en la tercera parte, se sintetizó un nuevo surfactante quiral, aunque debido a la duración limitada del proyecto, no se pudo completar la verificación de su efecto para lograr la quiralidad en las nanoestrellas de oro. El tensioactivo quiral se caracterizó mediante espectroscopia ^{1}H-NMR, ^{13}C-NMR y espectrometría MS.

Palabras clave: nanomateriales, nanopartículas de oro, nanoestrellas de oro, quiralidad, resonancia de plasmones superficiales, surfactante.

Schedule

February 2023

Sun	Mon	Tue	Wed	Thu	Fri	Sat
			1	2	3	4
5	6	7	8	9	10	11
12	13	14	15	16	17	18
19	20	21	22	23	24	25
26	27	28				

March 2023

Sun	Mon	Tue	Wed	Thu	Fri	Sat
			1	2	3	4
5	6	7	8	9	10	11
12	13	14	15	16	17	18
19	20	21	22	23	24	25
26	27	28	29	30	31	

April 2023

Sun	Mon	Tue	Wed	Thu	Fri	Sat
						1
2	3	4	5	6	7	8
9	10	11	12	13	14	15
16	17	18	19	20	21	22
23	24	25	26	27	28	29
30						

May 2023

Sun	Mon	Tue	Wed	Thu	Fri	Sat
	1	2	3	4	5	6
7	8	9	10	11	12	13
14	15	16	17	18	19	20
21	22	23	24	25	26	27
28	29	30	31			

June 2023

Sun	Mon	Tue	Wed	Thu	Fri	Sat
				1	2	3
4	5	6	7	8	9	10
11	12	13	14	15	16	17
18	19	20	21	22	23	24
25	26	27	28	29	30	

- Experimental procedures
- Analysis of the obtained results
- Bibliographic research
- Writing

1. Introduction

1.1 Nanotechnology

Nanotechnology is a field of science that focuses on the study and manipulation of materials between 1 and 100 nm in size. At this scale, materials show unique physical, chemical, and biological properties, which can be applied to create novel materials with enhanced properties and functionalities.[1]

Nanomaterials have been around for a long time, and it could be said that chemists have been working with them since the beginning of their fields, even though the term "nanotechnology" was only coined in the 1960s. In fact, NPs were utilized in Roman glass over 2000 years ago, where clusters of gold nanoparticles (Au NPs) were used to generate vivid colors.[2]

In the current century, the development of nanotechnology has revolutionized many industries, leading to the widespread use of nanomaterials (NMs), as is shown in Figure 1. Some relevant examples are, i) carbon nanotubes, which are used in electronics due to their unique electronic properties, ii) silicon and titanium dioxide, applied in solar cells to increase their efficiency and lower their cost, and iii) iron dioxide, which are used for water and soil remediation to remove pollutants and toxins.

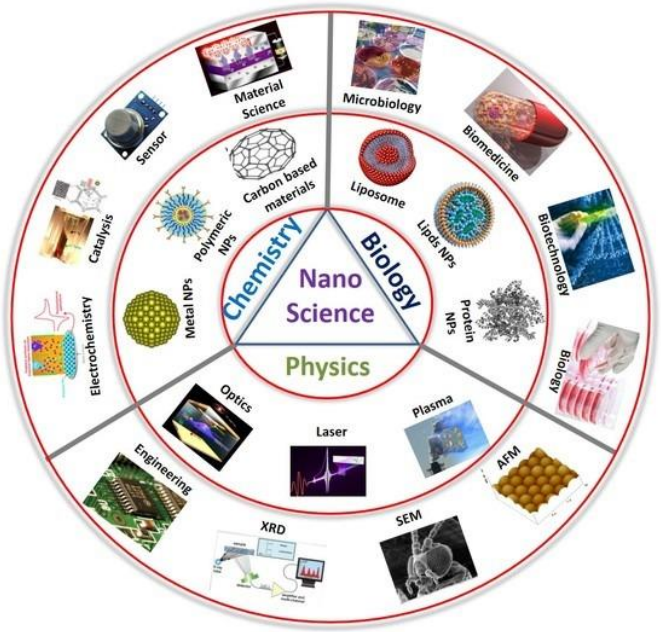

Figure 1. Contributions of nanotechnologies in different fields of science, including chemistry, materials science, physics, biology, computer science, and engineering.[3]

1.2 Plasmonic nanoparticles

Plasmonic NPs exhibit unique optical properties due to their ability to support localized surface plasmon resonances (LSPRs), which occurs when electromagnetic radiation excites free electrons in the metal. This excitation causes the collective oscillation of the electrons in the NPs, resulting in charge separation and dipole oscillation, as it is represented in Figure 2. The frequency at which the amplitude of the oscillation is maximum is known as the SPR frequency. The intensity of the SPR band depends on factors such as surface morphology, composition, temperature, dielectric environment, metal type, and particle size.[4]

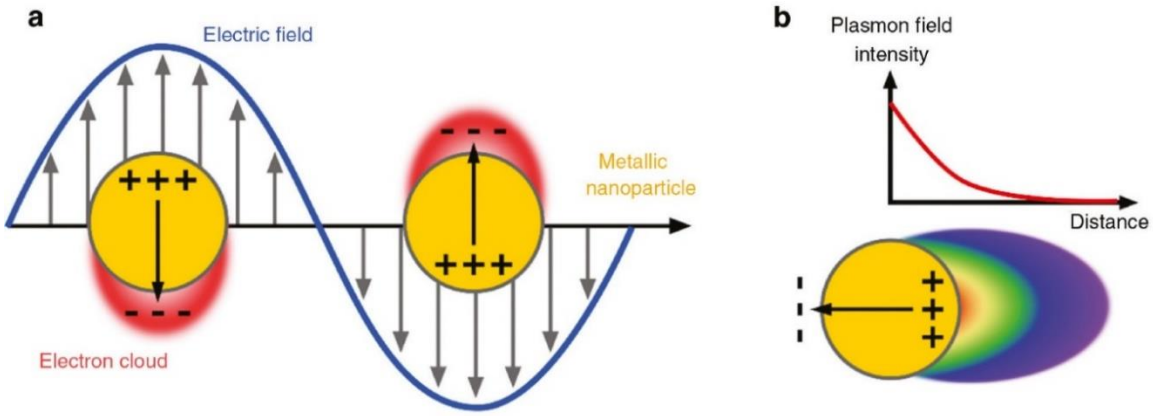

Figure 2. Interaction of metal NPs with light. (a) Schematic representation that demonstrates the impact of an incoming electromagnetic wave on the electron cloud surrounding a spherical NP. (b) Another schematic representation that portrays the decay of a plasmonic field as it moves away from the surface of the metal.[5]

By adjusting the size, shape, and composition of plasmonic NPs, their optical properties can be tuned to suit various applications, such as enhancing light absorption in solar cells, improving sensing capabilities in biosensors, or as catalysts for chemical reactions. The plasmonic property has made these NPs an attractive research topic in multiple areas, such as catalysis, electronics and sensors.

Although there are several plasmonic metals such as gold, silver, copper, or aluminum, only a limited number possess the ability to support plasmon resonances in the visible range of the electromagnetic spectrum. Additionally, some of these metals have low stability against oxidation. For these reasons, silver and gold are the most frequent metals applied for the preparation of plasmonic NPs.

One of the main applications of plasmonic NPs is the Surface-enhanced Raman scattering (SERS). SERS is a powerful vibrational spectroscopy technique that provides high sensitivity due to the enhancement of the Raman scattering signal of molecules located near plasmonic surfaces. This effect arises from the LSPR of plasmonic NPs, which produces strong and confined electromagnetic fields at the NP surface.

In plasmonic NPs, SERS hot spots can arise from two main factors. The first factor is the presence of sharp edges or tips on the NP surface, which can significantly enhance the electromagnetic field due to the strong SPR effect. The second factor is the hybridization of plasmon modes, which occurs when the plasmon resonances of closely spaced NPs interact. As a result, the SERS hot spots are situated within the gaps between the NPs.[6]

1.2.1 Gold nanoparticles

Gold is a noble metal known for its high stability, low reactivity, and low toxicity, making it an attractive material for the preparation of NMs. Au NPs have attracted significant attention due to their low toxicity that makes them suitable for use in various biomedical applications, such as the ones shown in Figure 3. Additionally, as it was mentioned previously, their plasmonic properties allow them to absorb and disperse light, enabling them to convert optical energy into heat through the process of nonradiative electron relaxation. For these reasons, they are currently used for targeted drug delivery, cancer therapy, and imaging.

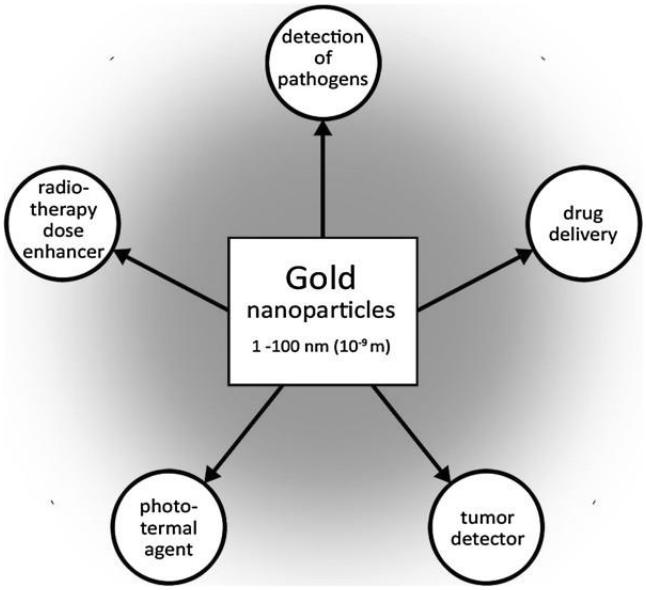

Figure 3. Common medical applications of Au NPs.[7]

Over the past few decades, a variety of colloidal-based approaches have been created to control the size, shape, and surface properties of Au NPs. One of the earliest and most widely used synthetic methods for producing Au NPs is the Turkevich method, which was established in 1951. In this method, citric acid is used as both a reducing and stabilizing agent for hydrogen tetrachloroaurate ($HAuCl_4$) in boiling water. By adjusting the gold-to-citrate ratio, the size of the resulting particles can be regulated, resulting in the production of dilute solutions of moderately stable spherical Au NPs with diameters ranging from 10 to 20 nm.

Nowadays, the colloidal synthesis of Au NPs is mainly performed in the presence of surfactants. These are amphiphilic molecules that have a hydrophobic tail and a hydrophilic head. When added to a solution containing Au NPs, surfactants adsorb onto the surface of the NPs, forming a protective layer that prevents them from aggregating. This layer also stabilizes the Au NPs, allowing for their manipulation and use in various applications.

To achieve narrow size and shape distributions in the colloidal synthesis of Au NPs, a strategy called seed-mediated synthesis is currently used. This strategy involves a spatial and temporal separation between the initial nucleation of nanocrystals from their subsequent growth. First, small Au NPs, or "seeds," are formed in a solution containing a reducing agent, a gold precursor, and a stabilizing agent. These seeds then act as nucleation sites for the growth of larger Au NPs in a separate solution, resulting in a more controlled and uniform size distribution.[8]

Au NPs are highly versatile in terms of their optical properties, as its interaction with light can be readily tailored by controlling their size and morphology. This has led to increasing research interest in the synthesis of Au NPs of different shapes and sizes over the past few decades.[9] The most studied shapes of Au NPs include:

- Gold nanospheres (Au NSs): The LSPR band of Au NSs starts to appear when their size is larger than a few nanometers, and it is typically in the visible region of the electromagnetic spectrum, ranging from 500 nm to 600 nm (Figure 4). As the diameter of the Au NSs increases, their LSPR peak shifts towards the longer wavelengths of the spectrum. For example, the plasmon band of spherical Au NPs with a diameter of around 20 nm is typically around 527 nm.[10]

- Gold nanorods (Au NRs): They have two distinct bands: a strong band in the near-infrared (NIR) region corresponding to electron oscillation along the long axis (longitudinal band), and a weak band in the visible region (transverse band). The longitudinal band is sensitive to aspect ratios, causing a red-shift and color change. This makes Au NRs suitable for phototherapy due to low tissue absorption in the NIR region.[11]

- Gold nanostars: They are highly anisotropic NPs with a small spherical core and a variable number of tips. They exhibit strong absorption in the NIR region due to plasmon interactions between the core and tips.[12] Typically, these nanostructures exhibit a plasmon band attributed to the core and several plasmon bands associated to the tips and core–tip interactions,[11] ranging from 500 to 1400 nm, as is shown in Figure 4. The exact positioning of these bands depends on the shape of the branches and their interaction with each other.[10] Their sharp tips create electromagnetic fields and hotspots, making them suitable for SERS and photothermal therapy. Gold nanostars amplify localized electric fields and are used in applications like SERS, data storage, and photo-excitation.[13] However, their susceptibility to reshaping and oxidation limits their range of applications. Although this can be partially solved by adding thiolated ligands with a high affinity for gold surface, this problem limited the range of applications for these structures.

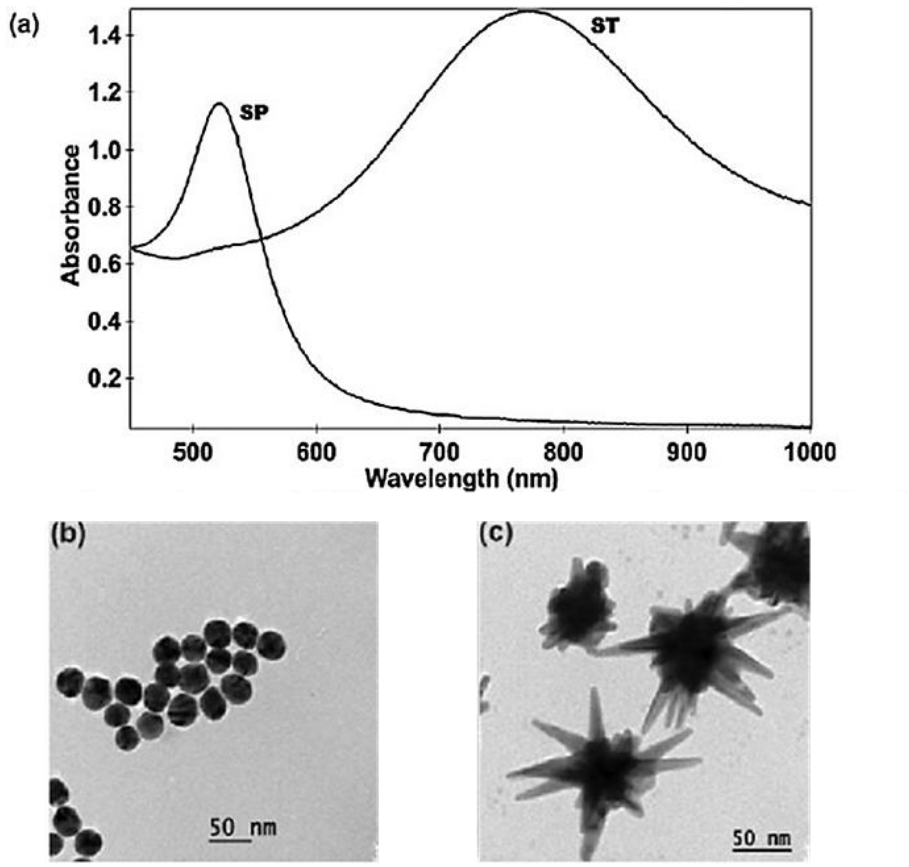

Figure 4. UV-VIS spectra and Transmission Electron Microscopy (TEM) images of gold nanospheres (SP, b) and gold nanostars (ST, c).[14]

1.3 Mesoporous silica nanoparticles

Silica NPs are formed by silica tetrahedra where four oxygen atoms are bound to one silicon atom, resulting in a three-dimensional network of interconnected silica. This material is typically amorphous in nature and can be prepared in a wide range of sizes and shapes. Its preparation typically consists of a sol-gel process where a silica precursor such as tetraethyl orthosilicate (TEOS) is hydrolyzed in the presence of water and an acid or base catalyst. The hydrolysis reaction results in the formation of silica oligomers, which then condense to form a three-dimensional network of interconnected silica.[15]

Silica NPs belong to a noteworthy class of NMs that have attracted considerable attention across diverse fields due to their unique properties. One of the main advantages of this material is that their surface chemistry can be straightforward

modified, allowing for their customization to specific applications. Another advantage is their biocompatibility, as they are generally considered to be safe for use in biomedical applications. Furthermore, silica NPs exhibit excellent water dispersibility, which facilitates its applications in aqueous environments.

Silica NPs can be categorized into different types, with two common types being nonporous and mesoporous. The primary distinguishing factor between these two types is that mesoporous silica nanoparticles (MSNs) contain pores, which are typically between 2 and 50 nanometers in size. The presence of the pores endows this material with a higher surface area. Additionally, the pores can be applied to encapsulate molecules or even perform catalytic processes.

The hexagonal arrangement of cylindrical mesopores within MSNs forms a highly organized structure of well-defined channels. Silica's simple polycondensation chemistry enables the covalent bonding of diverse functional groups, either during the material´s initial synthesis or through post-synthesis grafting. This approach provides precise control over the loading and positioning of functional groups. By modifying the mesoporous channels or the external particle surface with different functional groups, these materials can be manipulated to have various surface properties. This makes them useful for applications such as controlled release delivery and biosensing.[16]

Typically, mesoporous silica materials are synthesized using a technique called surfactant-templating, illustrated in Figure 5. This process involves the use of surfactant molecules, such as CTAB, as a template to direct the structure of the material, while TEOS is used as the silica source. The surfactant can be easily removed from the inorganic silica cast using mild extraction methods such as acid-dissolution, calcination, or solvent extraction. These procedures effectively eliminate the surfactant without causing any significant disruption to the silica structure.

The mechanism behind the formation of these materials is similar to the growth of metal NPs. Initially, the surfactant molecules assemble into micelles at their critical micelle concentration (CMC) in a basic medium. Then, silica is added, leading to nucleation and subsequent growth through cocondensation, resulting in uniform-sized structures made up of both organic and inorganic components.[17]

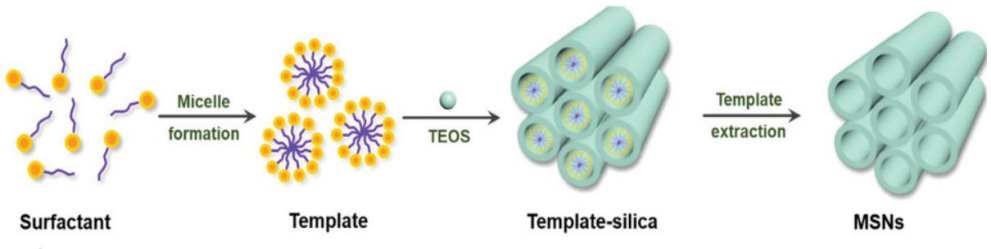

Figure 5. Schematic representation depicting the general process of MSNs formation using a cationic surfactant as a template.[17]

The structural characteristics of MSNs are determined by the composition of the precursor solution, particularly the concentrations of the surfactant and water. The formation of micelles and the CTAB molecules, which serve as templates, are influenced by these factors, thereby influencing the textural morphology of the MSNs. Other factors that influence MSN morphology include the source of silica, as well as the characteristics of copolymers or surfactants used as templates. Through manipulation of these parameters, it is possible control the hydrolysis rate, the extent of interaction between the templating agent and the silica polymer, as well as the condensation process of the silica precursor.

Particle size is strongly affected by stirring; a slow rate of stirring produces longer fibers. Pore size can be modulated by adjusting the quantities of silica source, surfactant, and the packing capacity of the surfactant. The presence of water affects in the aggregation, higher water content leads to elongation and growth of silica in accordance with the micelle structure. Dilution of the solution alters the arrangement of surfactant micelles, forming aggregates that encapsulate the silica source, reducing the hydrolysis of TEOS, and promoting the growth of the MSNs perpendicular to the pore alignment.[1819]

1.4 Gold-core silica shell nanoparticles

Gold-core silica shell nanoparticles (AuMSSs) are a type of hybrid nanoparticle that consists of a gold nanoparticle core surrounded by a layer of silica. These NPs have a unique structure that allows them to exhibit properties of both gold and silica, as the ones mentioned in Figure 6. For example, the plasmonic properties allow this hybrid material to strongly interact with light. On the other hand, the silica shell gives high colloidal stability and facilitates their functionalization. Importantly, both silica and gold are recognized as materials that are biocompatible, inert, and not toxic.[20,12]

Encapsulating Au NPs in nonporous silica oxide prevents direct contact with the surroundings, offering stability but limiting interactions. Mesoporous silica can overcome this by providing accessibility to the gold surface while maintaining protection. Mesopores enable selective accessibility based on molecule size, benefiting catalysis and SERS applications.

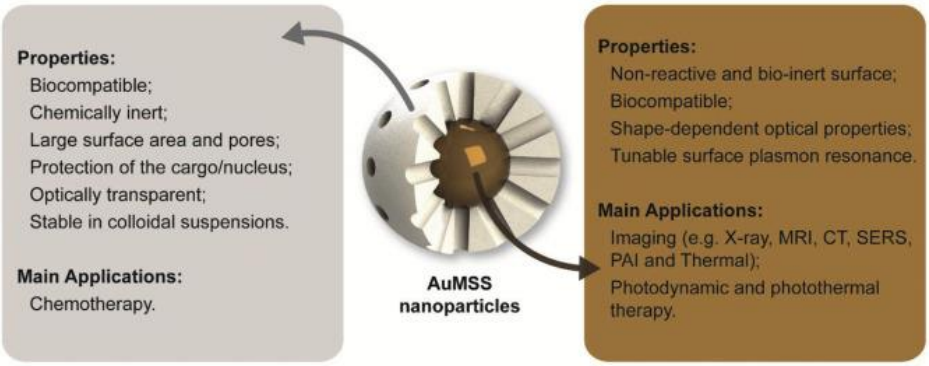

Figure 6. Properties and main applications of the two parts of the AuMSSs.[12]

The thickness of mesoporous silica shells can be controlled by adjusting the ratio of NPs to silica source. The synthesis method involves a surfactant-templated process derived from the Stöber method. These shells have radially extended pores determined by the size of the templating surfactant micelles. CTAB is commonly used as a surfactant, but other factors such as solvent, CTAB/TEOS ratio, temperature, stirring speed, pH, and reaction time affect pore organization and silicon oxide quality. However, pore size is mostly independent of reaction conditions as it is primarily determined by the micelles.[20]

The AuMSSs has also been applied to prepare Au nanostars with high stability. This can be done by growing Au tips from the central cores of silica-coated particles through the radial mesopores. This overgrowth reaction involves the reduction of $HAuCl_4$ in the presence of silver ions. The process by which the gold branches extend outward from the cores through the silica channels can be observed from 3D visualization of Au NSs tip growth in Figure 7.[20]

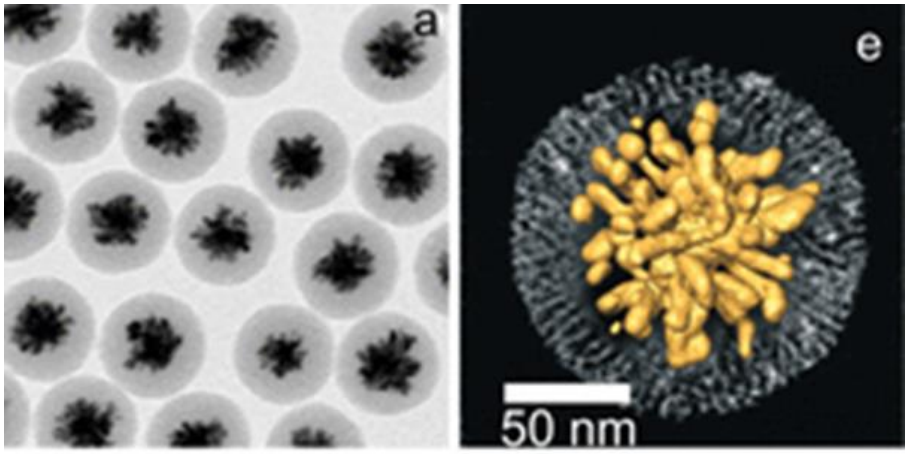

Figure 7. 2D and 3D (a, e) TEM images to characterize the hybrid nanostructures composed of Au NSs coated with mesoporous silica, after the growth of gold tips through the silica channels.[20]

The gold cores act as catalysts for gold reduction, leading to the preferential growth of gold branches over them. This fast reaction is typically completed within a few seconds, resulting in gold nanostructures with similar tip lengths. However, some variations in tip length can occur due to differences in the reaction rate. Aggregation of the nanostructures is only observed when the concentration of seed particles is insufficient, allowing the tips to reach the surface of the silica shell and form connections with neighboring particles.[20]

1.5 Chirality

Chirality is a concept that can be observed across all scales of our world, ranging from the form of galaxies to the structure of individual molecules. The word "chirality" comes from the Greek word for hand, "kheir," and is used to describe any object that cannot be perfectly overlapped with its mirror image. In 1848, Louis Pasteur discovered that chirality is a key feature of molecular systems. Since then, fundamental and technological advancements have significantly improved our understanding of chirality at the molecular level, as well as its importance in biological systems. Likewise, imparting handedness to plasmonic NPs has received considerable attention because it may provide important advantages for;[21]

1) The application of NPs in medicine.

2) The detection of biomolecules.

3) The design of enantioselective catalysts.

4) The fabrication of systems with a strong differential optical response to left and right circularly polarized light.

5) The preparation of nanocomponents similar to their macroscopic dissymmetric counterparts such as springs, gears and propellers. These chiral nanostructures may be essential components in the emerging field of nanorobotics.

The generation of chiral plasmonic NMs can be achieved by mainly two methods: organization of achiral plasmonic elements into a structure with a defined handedness, and the synthesis of individual plasmonic NPs with dissymmetric geometry.

1.6 Chirality in extrinsic plasmonic nanoparticles

To date, dissymmetric assemblies have been by far the most applied strategy to fabricate chiral plasmonic NMs. These assemblies mainly originate from the utilization of molecular self-assembly techniques to arrange non-chiral plasmonic NPs in a chiral manner, where the interactions between the dipole moments of the individual nanoparticles result in the emergence of coupled collective SPR modes.

To fabricate the chiral assemblies bottom-up strategies such as self-assembly methods are used. These approaches use either chemical or physical forces to organize individual building blocks into hierarchically structured ensembles. Self-assembly methods offer exceptional flexibility in controlling the structure, enabling the customization of chiroptical properties through template programmability or assembly process adjustability. However, the resulting circular dichroism (CD) spectra of chiral plasmonic nano-assemblies can be complex due to the presence of multiple modes that may overlap spectrally, leading to intricate spectral features.

In particular the following methods, illustrated in Figure 8, have been used to prepare chiral plasmonic nano-assemblies: (1) Integrating plasmonic NPs onto a pre-existing chiral template, such as such as e-beam-lithography-patterned thin films, polymers,

nanofibers, or biomolecules. The chiral spatial organization of the nanoparticles is dictated by the template's inherent chirality. (2) Functionalizing with oligomeric scaffolds that promote their assembly into chiral structures through interactions resembling those found in macromolecules or supramolecular systems. (3) Applying external physical forces, such as mechanical stretching, shear forces, or light during or after the assembly to break the symmetry and induce anisotropy.[22]

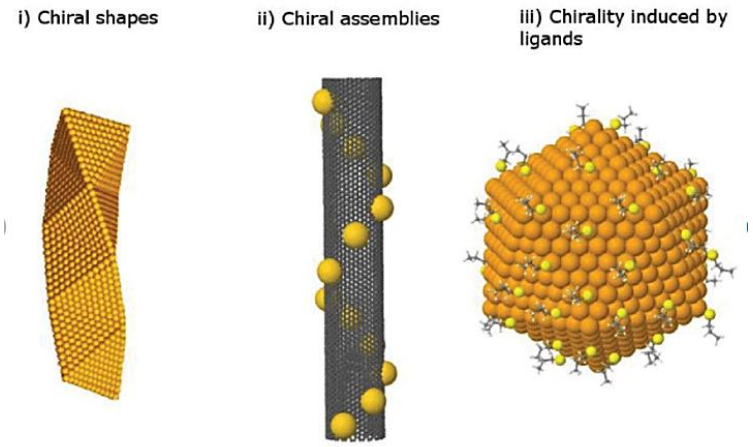

Figure 8. Three factors that contribute to chirality in nanostructures. (i) Intrinsic chirality resulting from the helical structure of an Au tetrahedral nanowire. (ii) Chirality induced by the assembly of Au NPs on a carbon nanotube. (iii) Chirality emerging from the asymmetrical arrangement of ligands on the surface of a symmetrical cluster.[23]

1.7 Chirality in intrinsic gold nanoparticles

Advances in the colloidal synthesis of noble metal NPs achieved during the past decades has allowed the production of plasmonic NPs with diverse morphologies, including chiral ones. In order to achieve this, a molecule or biomolecule, such as an amino acid, is employed as a template during the synthesis of NPs. Notably, Nam's group has made remarkable advancements in this field. They have successfully synthesized what are known as "plasmonic helicoids" with intricate twisted structures derived from cubic or octahedral nanoparticle seeds. These unique morphologies are achieved using enantiomers of cysteine and glutathione, which act as chiral inducers. Figure 9 illustrates the results of their research.

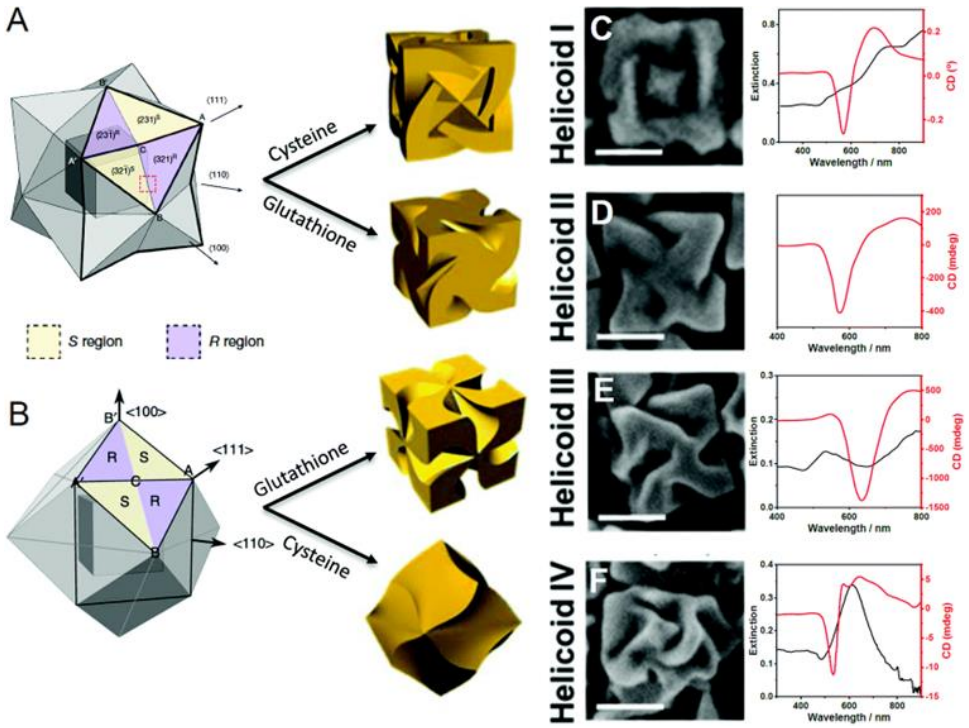

Figure 9. (A and B) Schematic representation of a star-shaped eight-faced polyhedron (A) and a diamond-shaped twelve-faced polyhedron (B), characterized by surfaces composed of S region and R region configurations. Upon exposure to cysteine and glutathione, these nanostructures undergo a transformation into various spiral forms, as indicated in (C–F). Representative scanning electron microscopy (SEM) images and the corresponding UV-vis and circular dichroism (CD) spectra of: 432 Helicoid I (C), 432 Helicoid II (D), 432 Helicoid III (E), and 432 Helicoid IV (F).[24]

A conceptually different approach, recently showcased by Liz-Marzan, involves using chiral co-surfactants to facilitate the development of Au NRs with spiral-shaped helical characteristics. This technique consists of applying chiral co-surfactants like 1,1′-bi(2-naphthol) (commonly known as BINOL) and 1,1′-binaphthyl-2,2′-diamine (BINAMINE) in combination with a quaternary ammonium surfactant (CTAC). A qualitative analysis of the chiral features of the Au NRs obtained by this method is shown in Figure 10. By combining specific molecules, such as enantiomers of a co-surfactant, with pre-formed Au NRs, researchers have successfully achieved chiroptically active micelles with unique worm-like structures. These micelles exhibit a quasi-helical pattern as they adhere to the Au NRs, effectively serving as templates for guided seed-growth. As a result of this process, distinct and pronounced wrinkles are formed on the Au NRs surfaces. Importantly, the handedness of these wrinkles is determined by the specific enantiomer of the co-surfactant employed during the growth process.[24]

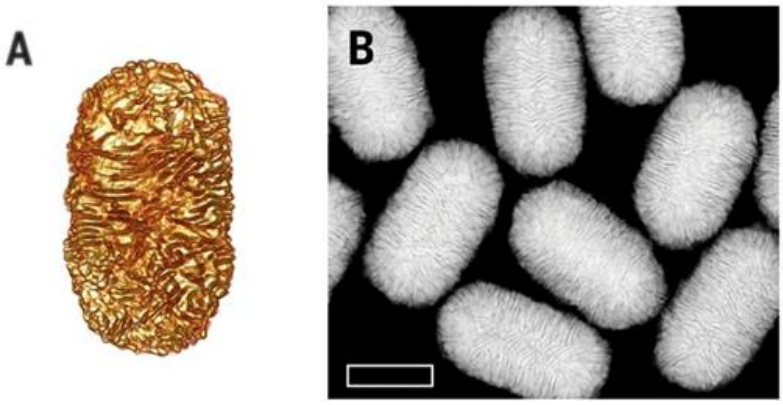

Figure 10. Qualitative analysis of chiral features of Au NRs. (A) The three-dimensional structure of an Au NR that was grown in the presence of an (R)-BINAMINE-surfactant mixture. Additionally, a low-resolution high-angle annular dark-field scanning transmission electron microscopy (HAADF-STEM) image (B) was captured to provide further insights into the chiral properties of the Au NRs. Scale bar, 100 nm.[25]

2. Objectives

The overall objective of this undergraduate project is to develop a synthetic methodology for the preparation of a novel type of chiral plasmonic NPs, i.e., gold nanostars with chiral branches. This objective will be achieved by following the strategy illustrated in Figure 11.

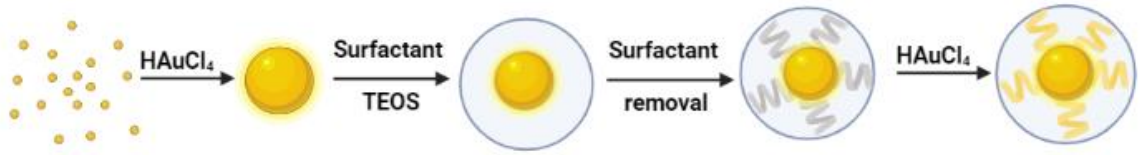

Figure 11. Schematic representation for synthesizing gold nanostars with chiral branches.

To accomplish this main goal, the following specific steps will be undertaken:

1. Replication of the gold nanostar synthesis based on AuMSSs as reported by N. Sanz-Ortiz M et al.[20] This step involves reproducing the previously published synthesis method for achiral gold nanostars using AuMSSs.

2. Evaluation of the chiral surfactant's **CS1** (Figure 12) capability to induce chiral mesoporosity in AuMSSs.

3. Synthesis of another chiral cationic surfactant, **CS2** (Figure 12) as an alternative to CTAB in the previously established synthetic method that could induce chiral mesoporosity in AuMSSs for future studies.

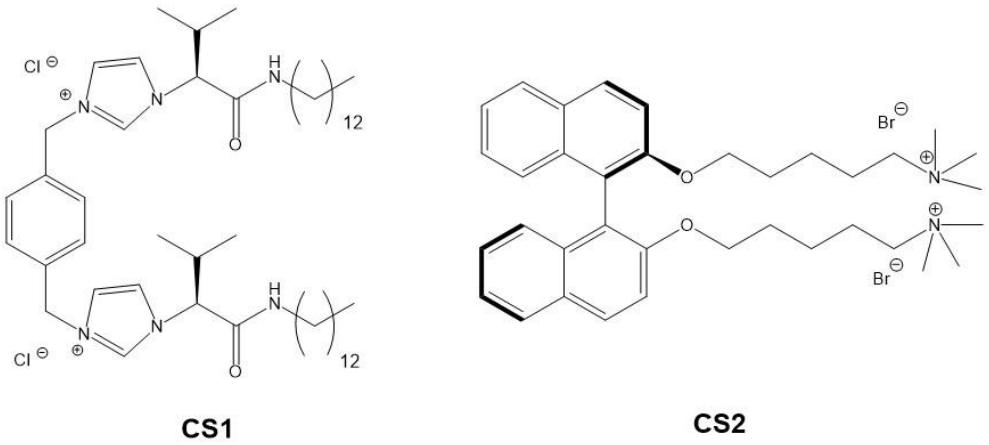

Figure 12. Structures of the chiral surfactant used for the experiments (**CS1**) and the one synthesized for future ones (**CS2**).

3. Experimental procedure

3.1 General experimental procedure

All the chemicals used in the experiments were bought as reagent grade and used without further purification. MilliQ water was obtained from a Direct-Q 5 UV water purification system. All the material used in the synthesis of Au NPs was previously washed with aqua regia (3 parts HCl, 1 part HNO_3), rinsed with MilliQ water, and then oven-dried at 60°C.

Synthesized Au NPs in all steps were characterized by UV-Vis spectroscopy, to obtain their Au^0 concentration and LSPR band to confirm their geometry, and by TEM for the monitoring of the change in shape in each step.

Au NPs solutions can be characterized by UV-Vis spectroscopy because they exhibit a characteristic UV–Vis extinction spectra due to the presence of a LSPR signal in the visible part of the spectrum. The size of Au NPs and the molar concentration of Au^0 can be extracted directly from this spectrum.

The determination of the concentration for all UV–Vis were done at an absorbance wavelength of 400 nm, which enabled to obtain an accurate determination of Au^0 concentration, since this wavelength is located between two decisive spectral regions: below 400 nm, the absorbance is influenced by organic substances, such as commonly used stabilizers; and above 400 nm, the absorbance is affected by the LSPR of the Au NPs, which also depends on their size and shape.

The primary functionality of the Abs_{400} method in determining the concentrations of Au^0 is based on the permissible interband transitions occurring at 3.1 eV, specifically the transitions from 5d to 6sp in bulk gold. At room temperature, direct interband transitions at this energy level are allowed. As a result, the Abs_{400} measurement exhibits a linear relationship with the Au^0 concentration, potentially enabling its direct quantification.[26] Once the absorbance is known, Au^0 concentration is calculated with Lambert-Beer´s law:

$$[Au\ NPs] = \frac{Abs_{400}}{\varepsilon \cdot \mathrm{b}}$$

Being A_{400} the Au^0 absorbance at 400 nm, ε the extinction coefficient of Au NSs (0.0005 M^{-1} cm^{-1}) and b the optical path length (1 cm).

UV-Vis spectra were measured in a GENESYS 50 UV-Vis Spectrophotometer and TEM images were obtained in a JEOL JEM-1010 electron microscope at an acceleration voltage of 100 kV. Samples for TEM analyses were prepared by adding a single drop (20 µL) of the different solutions of Au NPs onto a copper grid coated with a carbon film (200 mesh, Electron Microscopy Sciences). The grid was left to dry for several minutes at room temperature.

Chiral surfactant **CS1** used for experiments was provided from the Department of Inorganic and Organic Chemistry, ESTCE, University Jaume I, Castellón, Spain. Its CMC value is 2 mM in a mixture of water/methanol 1:1.[27]

The chiral surfactant synthesized was characterized by ^{13}C-NMR and ^{1}H-NMR spectroscopy and ESI-MS spectrometry. Reactions were monitored by thin-layer chromatography (TLC) using thin layer plates Scharlau Aluminium Si UV254.

NMR and MS spectra were carried out at Servizos de Apoio á Invertigacion (SAI), from Universidade of A Coruña (UDC). NMR spectra were done using a Bruker AVANCE 500 spectrometer (300 MHz in the case of ^{1}H-NMR and 126 MHz for ^{13}C-NMR). MeOD was used as solvent. All chemical shifts (δ) are reported in parts per million (ppm) and coupling constants (J) in hertz (Hz). ESI-MS spectrum was measured on an Orbitrap LTQ Discovery mass spectrometer.

Organic product purifications were carried out by MPLC in a BUCHI Pure C-810 Flash using a 20 g reverse phase ultra-aqueous C18 column.

3.2 Synthesis of the achiral Au nanostars

3.2.1 Synthesis Au seeds

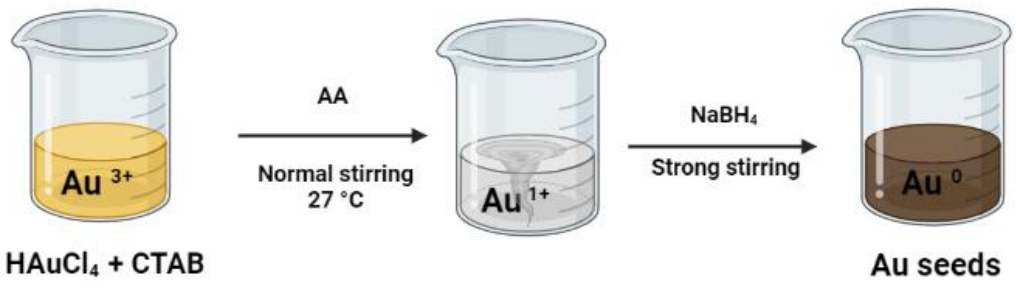

Au seeds were synthesized by using a modification of the method reported by González-Rubio et al.[28] By employing this seed-growth method, the NPs enlarge step by step, so that it becomes easier to control the sizes and shapes of the Au NPs.[11]

200 µL $HAuCl_4$ (50 mM) were added to 35 mL of CTAB (100 mM) in a 50 mL glass beaker at 27°C, with a magnetic stirrer bar that covered all the area of the bottom of the beaker. Upon addition, the solution exhibited an orange-yellow color, indicating the presence of Au^{+3} ions. Then 140 µL of an aqueous ascorbic acid (AA) solution (100 mM) were introduced into the reaction mixture and it turned colorless due to the formation of Au^{+} ions. Finally, 800 µL of freshly prepared $NaBH_4$ (20 mM) were added instantaneously after increasing the magnetic stirring to create a whirlwind-like motion. As $NaBH_4$ reacted with the Au NPs, the solution quickly transformed from colorless to brown, confirming the successful reduction process. The reaction mixture was left for 30 min to remove excess of $NaBH_4$. Here AA and $NaBH_4$ act as capping and stabilizing agents for Au NPs.[29]

3.2.2 Synthesis Au NSs

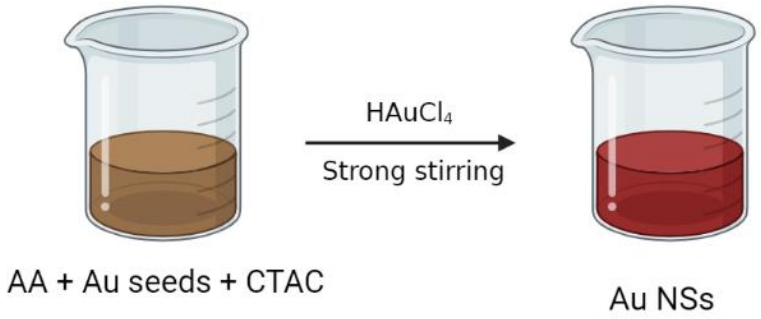

In a 1 L glass beaker, a solution was prepared by combining 200 mL of CTAC (200 mM), 150 mL of a 100 mM aqueous AA solution and 5 mL of Au seeds. The CTAC solution appeared clear prior to the addition. 200 mL of $HAuCl_4$ (2 mM) was swiftly introduced into the beaker under vigorous stirring. The rapid addition and strong stirring facilitated the reaction kinetics. As a result, the solution underwent a remarkable color change from brown to a deep red wine hue. This alteration in color indicated the successful reduction of gold ions and the formation of Au NSs.

For the purification, three centrifugation cycles were done (1h 30',17000 rpm). First, 35 mL of Au NSs solution were redispersed in water to a final concentration of 30 mM. Then they were centrifugated two more times and redissolved in CTAC 10 mM. The supernatant was retired and 5 mL of CTAC 0.1 M were added into each Falcon tube, then all the content of the tubes poured into a plastic bottle and stored in the fridge.

With UV-Vis the concentration of gold in the solution was determined, being [Au] =2.1 mM. Since it was needed more concentrated for the next step, 8 mL of the red wine solution were centrifugated (30', 13000 rpm), 1 mL of CTAB 10 mM was added and the new concentration was [Au]= 5.7 mM.

3.2.3 Synthesis mesoporous silica-coated gold particles

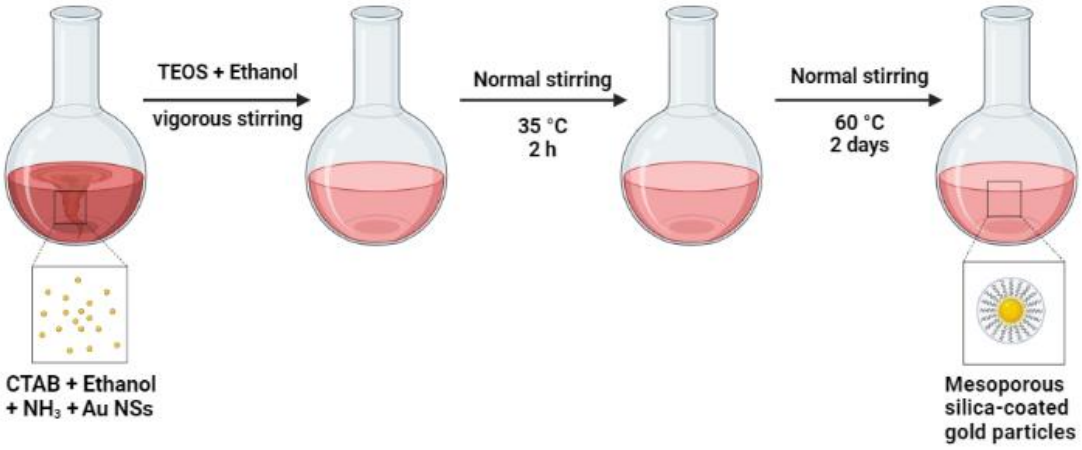

In a 250 mL round-bottomed flask, a solution was prepared using optimized conditions based on the method described by N. Sanz-Ortiz et al.[20] The flask was initially charged with 72 mL of CTAB (4.3 mM), 26 mL of ethanol (26 vol%), and 33 µL of NH_3 stock solution (30 vol%). To this mixture, 1.7 mL of Au NSs (5.7 mM, 0.1 mM in the total reaction volume) was added, resulting in the formation of a dark red solution.

Then the flask was placed in a silicone bath at 30-35 ºC with magnetic stirring. After 5 min of stirring, a solution of 100 µL TEOS + 100 µL ethanol was added dropwise increasing the stirring, and the reaction solution turned lighter red. After 2 h it was moved to a bath at 60 ºC and left in the lab for 2 days, remaining the same color.

For the purification, 24 mL of this solution were once centrifugated (30', 9000 rpm) and then washed with 1 mL of ethanol in the same conditions.

For the elimination of the surfactant encapsulated on the pores, after the supernatant (ethanol) was discarded, 1 mL of HCl (1 M) in ethanol was added, it was stirred for 5 min and the solution was centrifugated (30', 9000 rpm). Then it was washed two times with 1 mL of ethanol to remove any excess of HCl in the same conditions and redispersed in 200 µL of MilliQ water to have [Au]=1.2 mM for the next step.

3.2.4 Branching through silica pores

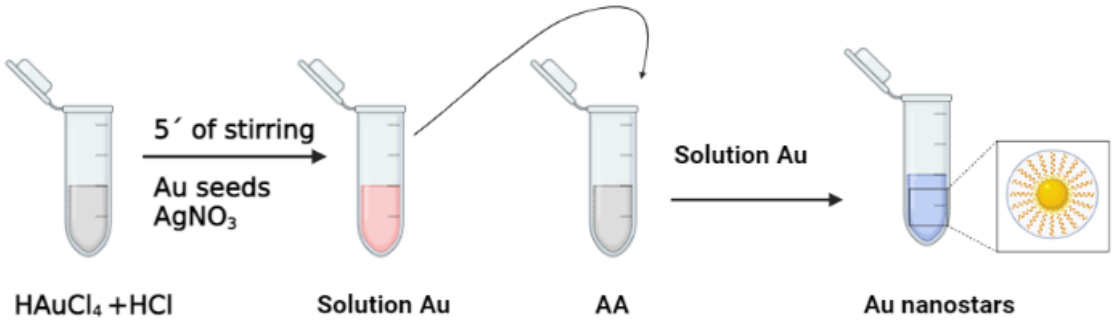

Based on the procedure described by N. Sanz-Ortiz et al.,[20] the following steps were followed. In a 2 mL Eppendorf tube, a solution was prepared by combining 3 µL of $HAuCl_4$ (0.25 mM) and 1 µL of HCl (1 M). The solution was stirred for 5 minutes. Subsequently, 40 µL of Au seeds from the previous step (1.2 mM) and 10 µL of $AgNO_3$ (3 mM) were added to the Eppendorf tube, following a specific order, and shaking after each addition. This red solution was added in another Eppendorf of 2 mL containing 5 µL of a transparent AA solution (0.1 M) and the final solution turned blue-gray, as is illustrated in the reaction scheme above.

The final solution was allowed to rest undisturbed for 10 minutes to facilitate any additional reactions or stabilization processes. For the purification they were centrifugated once (20', 9300 rpm) and redispersed in 700 µL milliQ water.

3.3 Synthesis nanostars with chiral surfactant

3.3.1 Synthesis mesoporous silica-coated Au NSs

In order to grow the silica coating, the same procedure as in the synthesis of the achiral nansotars was done, following the paper reported by N. Sanz-Ortiz M et al.[20] with several modifications to the quantities of the reactants, since the final volume was 2 mL.

To establish a control and determine the minimum amount of CTAB required to grow chiral nanostars, a series of experiments were conducted (Table 1), varying the proportions between CTAB and a chiral surfactant, **CS1**, whose structure is shown in Figure 13. Furthermore, a control using only CTAB (**LS12**) was conducted in order to

identify any issues. Experiments with only **CS1** were not carried out as the Au NPs aggregate and precipitate.

Table 1. Experiments with different concentrations of surfactants for the control of the amount of CTAB required to assess stability.

Experiment	[CS1] (mM)	[CTAB] (mM)
LS10	2.00	0.00
LS11	0.25	3.75
LS12	0.00	4.00
LS13	0.10	3.90

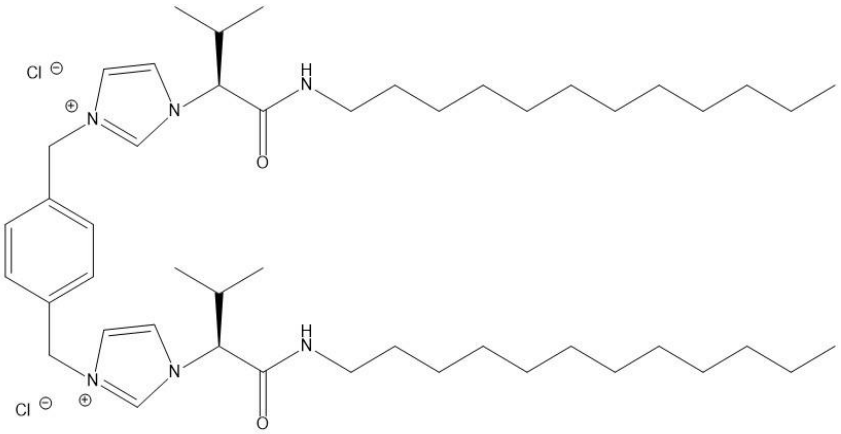

Figure 13. Structure of **CS1** used for the synthesis of chiral gold nanostars.

Other parameters were kept constant in all experiments, like the amount of TEOS/Ethanol solution (2 µL, 4.5 mM), the Au^0 concentration (43 µL, 0.1 mM) and the amount of ethanol (520 µL, 26 % m/v) and NH_3 (0.7 µL, 30 % m/v). The amount of MilliQ water added was the necessary to complete a final volume of 2 mL in each experiment.

For the purification, all samples were once centrifugated (30', 9100 rpm) and then washed two times with 1 mL of ethanol each (20', 9500 rpm). The resulting pellets were then redissolved in ethanol; in 200 µL the CTAB control, and in 50 µL the rest of experiments that were going to be used for TEM analysis.

3.3.2 Synthesis chiral nanostars with variations

As the previous experiments were not successful, the same experiments with **CS1** were done but varying the silicon source in the step where the TEOS solution in ethanol is added. The two variations, and its structures (in Figure 14) were:

1) TEOS/ 3-(triethoxysilyl)propane-1-thiol (Thiol) 2 % and 5 % with respect to TEOS.

2) TEOS/ (3-Aminopropyl)iethoxysilane (APTES) 5 % and 10 % with respect to TEOS.

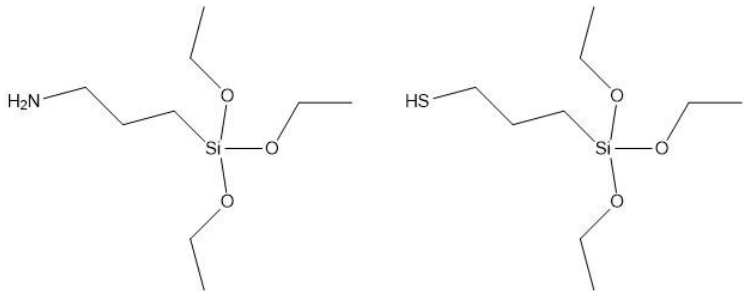

Figure 14. APTES and Thiol structures, respectively.

The same procedure as in the synthesis of the achiral and chiral nansotars was done, replicating the paper reported by N. Sanz-Ortiz M et al.[20] with several modifications. In addition, the proportion of surfactants was the same for all experiments represented in Table 2; **CS1** (0.1 mM) and CTAB (3.90 mM).

Table 2. Amount of different silica sources in the experiments to synthesize chiral gold nanostars.

Experiment	Thiol	APTES	% Thiol or APTES
LS16	X		2
LS17	X		5
LS18		X	5
LS19		X	10

For the purification, they were once centrifugated (30', 9500 rpm) and washed two times with 1 mL of ethanol (25', 9700 rpm) and redissolved in 200 µL of ethanol to be seen with TEM.

3.4 Synthesis of the chiral surfactant CS2

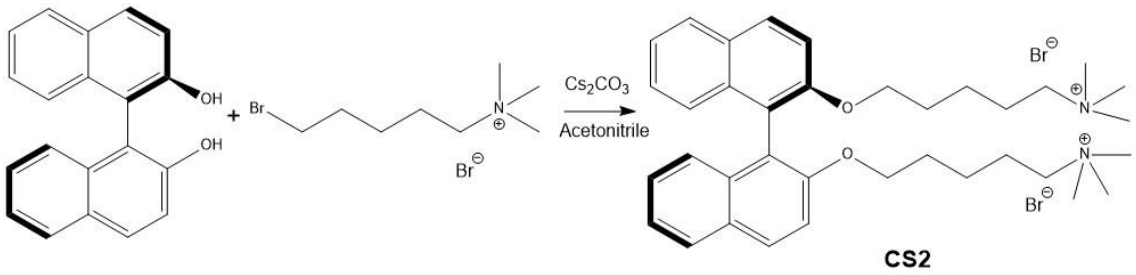

Since the previous experiments with the chiral surfactant **CS1** were not successful, a new surfactant with axial chirality called **CS2** was synthesized to be used in future studies.

(R)-[1,1'-binaphthalene]-2,2'-diol (BINOL) (700 mg, 2.44 mmol, 1.00 eq) was placed in a round bottom flask of 50 mL previously purged with N_2, covered with a septum and with magnetic stirring. Acetonitrile (17 mL, 150 mM) was added under a nitrogen atmosphere with a syringe, and it was dissolved forming a transparent solution. Then cesium carbonate (3.58 g, 11 mmol, 4.5 eq.) was added, which made the solution turn fluorescent yellow and finally 5-bromo-N,N,N-trimethylpentan-1-aminium bromide (2.83 g, 9.78 mmol, 4 eq.) was added. It was left refluxing at 85 °C overnight.

The next day, the product looked dark yellow and some white solid had appeared. The reaction was stopped and allowed to cool down to room temperature. Then it was filtered by vacuum and monitored by TLC (methanol/dichloromethane, 10:90 and revealed by a UV lamp). This technique showed that no unreacted reagent remained and all BINOL turned into the desired product.

The solvent was evaporated in the rotatory evaporator, obtaining a yellow solid. Then the product was dried under vacuum with a pump, obtaining a gold solid named **CS2** with a 59% yield.

CS2 was purified by MPLC in reverse phase, so that the desired product, being the most polar compound present, came out first. For the preparation, 200 mg of the surfactant were dissolved in 1 mL MilliQ water and the pure compound came out with metanol/water 1:3.

^{1}H-NMR (300 MHz, MeOD) δ (ppm): 8.37 (d, J = 9.0 Hz, 2H), 8.30 – 8.24 (m, 2H), 7.90 (d, J = 9.0 Hz, 2H), 7.69 (ddd, J = 8.1, 6.7, 1.2 Hz, 2H), 7.55 (ddd, J = 8.2, 6.7, 1.3 Hz,

2H), 7.43 – 7.36 (m, 2H), 4.48 – 4.29 (m, 4H), 3.31 (s, 18H), 3.29 – 3.20 (m, 4H), 1.91 – 1.78 (m, 4H), 1.72 (dq, J = 9.6, 7.2 Hz, 4H), 1.35 – 1.22 (m, 4H).

^{13}C-NMR (126 MHz, Methanol-d4) δ (ppm): 155.93 (2C), 135.43 (2C), 130.84 (2C), 130.51 (2C), 129.17 (2C), 127.30 (2C), 126.43 (2C), 124.79 (2C), 121.65 (2C), 117.01 (2C), 70.39 ($2CH_2$), 67.5 ($2CH_2$), 53.5 ($6CH_3$), 29.7($2CH_2$), 23.8 ($2CH_2$), 23.2 ($2CH_2$).

MS (ESI): calculated m/z for $[C_{38}H_{54}Br_2N_2O_2]^+$: m/z: 271.193, obtained: 271.200 (100.0%)

4. Results and discussion

4.1 Synthesis achiral gold nanostars

A five-step synthesis procedure depicted in Figure 15 was done, each step will be described in detail below:

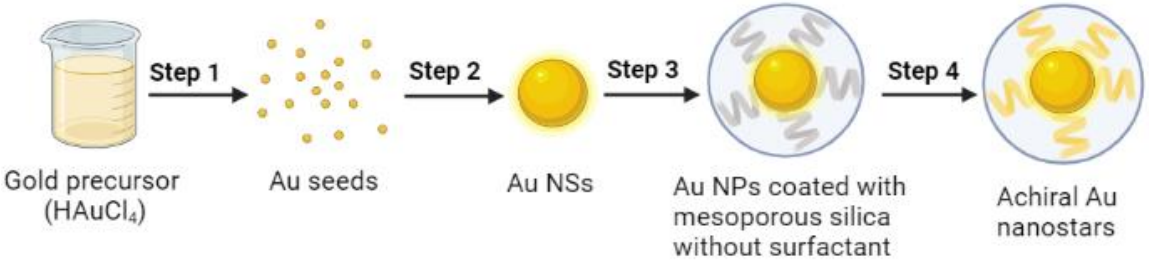

Figure 15. Schematic representation for synthesizing gold nanostars. In the first step, $HAuCl_4$ in CTAB was used as a gold precursor, and Au^{3+} is reduced to Au^0 seeds by AA and $NaBH_4$. In the second step, these Au^0 seeds were grown to give Au NSs by the addition of more $HAuCl_4$, AA and CTAC. The third step was the growth of the mesoporous silica coat around the particles, for which it was added CTAB, ethanol and NH_3 in the needed proportions, and then a mixture of TEOS and ethanol. Then the surfactant was eliminated, by washing with HCl in ethanol. Finally, in the fourth step, gold was branched through the silica pores, adding more $HAuCl_4$, HCl, $AgNO_3$ and AA.

4.1.1 Step 1

First, $HAuCl_4$ in CTAB was used as a gold precursor, in which gold was reduced by AA from Au^{3+} to Au^{1+}. In a medium with a high concentration of CTAB, this soft reducing agent lacks the necessary strength to effectively convert Au^{3+} ions to Au^0. [30] Subsequently, $NaBH_4$ was added to reduce from Au^{+1} to Au^0, giving rise to Au^0 seeds. By doing the reduction in two different steps, more homogeneity is ensured.

The seeds were characterized by UV-Vis spectroscopy (Figure 16), showing a spectrum identical to the one reported by Picciolini, S et al.[31] There is no sign of the plasmonic peak in the region between 500 and 520 nm that characterizes plasmonic NPs, so it demonstrates that the dimension of the seeds is less than 5 nm. Moreover, the solution obtained was brown, which also coincided with the paper reported by González-Rubio et al.[28]

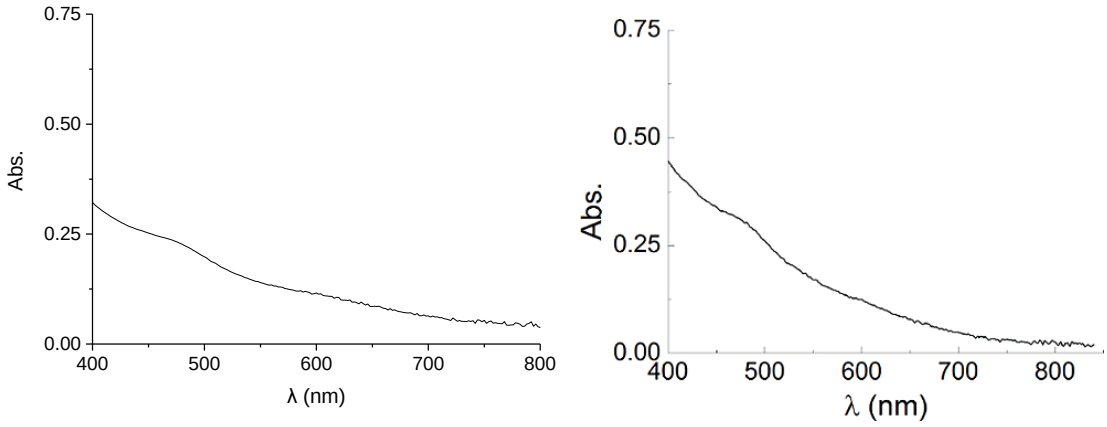

Figure 16. UV-Vis spectra of the experimental Au seeds on the left and bibliographic one [31] on the right.

4.1.2 Step 2

In the second step, Au^0 seeds were grown to give Au NSs by the addition of more $HAuCl_4$, AA and CTAC. By enlarging the particles step by step, it becomes easier to control the sizes and shapes of the Au NPs, allowing to obtain more monodispersed ones. The growing of the seeds is perceived through a change in color in the solution from brown to red wine.

The UV-Vis spectrum of the Au NSs (Figure 17) showed that they exhibit their LSPR band in the range of 500-550 nm as it was previously stated in the Introduction, specifically their maximum peak is at 520 nm. When the diameter of NPs is between 12 and 41 nm, the maximum absorption peaks locate at 520–530 nm, and as the diameter increases, this band is moved towards the red end of the spectrum. At exactly 520 nm, the diameter of Au NPs is around 12 nm.[32]

Moreover, the band decreases steeply, confirming that there is no aggregation between the particles. It is important to emphasize that the aggregation of Au NPs typically results in a red shift of the surface plasmon resonance (SPR) wavelength, accompanied by a broadening of the band, leading to a visible change in the color of the particles from red to blue[29], as demonstrated in Figure 17. This observable color transformation in the solution is primarily attributed to the coupling between the plasmons of the closely spaced particles.[33]

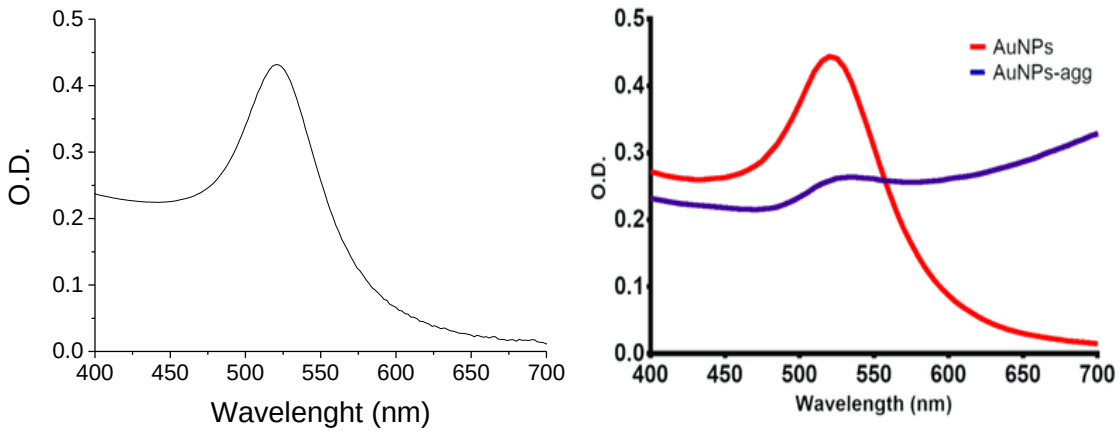

Figure 17. Experimental absorption spectrum of Au NSs (left) and bibliographic one (right) illustrating aggregated (AuNPs-agg) and non aggregated (AuNPs). The occurrence of aggregation leads to a noticeable shift in the intensity peak of the absorption spectrum, which subsequently results in a corresponding change in colorimetric properties.[34]

The achievement of Au NSs could also be confirmed by TEM images. The software *ImageJ* was utilized to accurately determine the size of several selected Au NSs. The results of Figure 18 revealed an average diameter of approximately 10±6 nm for the Au NSs.

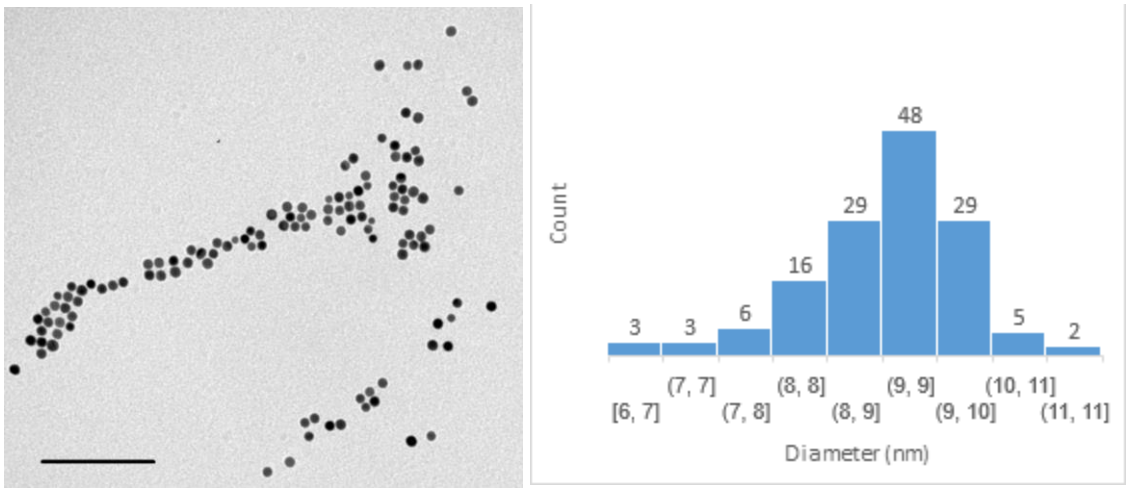

Figure 18. TEM image of purified Au NSs, scale bar 100 nm and histogram with normal dispersion of sizes of the Au NSs.

After their synthesis and purification, Au NSs were stored in CTAB because they are stabilized by its micelles, since this surfactant stabilizes metallic NPs in solution in an electrostatic and steric way. The presence of a cationic surfactant with elongated chains

and a polar head group facilitates the formation of a surfactant bilayer surrounding the NPs. This bilayer structure plays a crucial role in providing steric repulsion forces between the NPs, effectively preventing their agglomeration. As a result, a stable system is established, giving rise to a mutual stabilization system.

4.1.3 Step 3

The third step was the growing of the mesoporous silica coat around the particles, for which the synthesized Au NSs were used, and it was added CTAB, ethanol and NH_3 in the needed proportions, and then a mixture of TEOS and ethanol. Afterwards, the surfactant was eliminated, by washing with HCl in ethanol.

Here NH_3 is used to create basic media, with a pH around 10, for the hydrolysis of TEOS, the silica precursor. TEOS is not soluble in water, so ethanol must be also added. The capping surfactant (CTAB) is used as a template for the formation of the porous shells.

Then there was a washing step with HCl to eliminate surfactant from the pores. CTAB, a cationic surfactant, is employed with acid due to the negative charge of the silica layer´s pores caused by deprotonated silanol groups, which have a pKa of around 7,[35] resulting in a strong interaction with the cationic micelles. When HCl is added, it protonates the oxygens weakening the interaction between the surfactant and the silanol pores and therefore eliminating the surfactant from the mesoporous channels where the branches will be grown in the next step.

An UV-Vis spectrum was done to characterize the coated NPs before and after the elimination of surfactant (Figure 19), and it showed that the LSPR band characteristic for the Au NPs in the range of 500-550 nm was still present in both steps. The silica layer does not have significant absorption in the UV-Vis range and neither CTAB encapsulated in the pores, but because the Au NPs are in a different environment from the step before, their LSPR band is a little shifted to higher wavelengths. The Au NPs coated with silica exhibit a peak wavelength of 536 nm, while the removal of the surfactant results in a peak at 528 nm.

TEM images in Figure 19 showed the Au NPs coated with mesoporous silica. The results revealed with *ImageJ* showed an average diameter for 10 selected NPs coated with a mesoporous silica layer of approximately 50 nm.

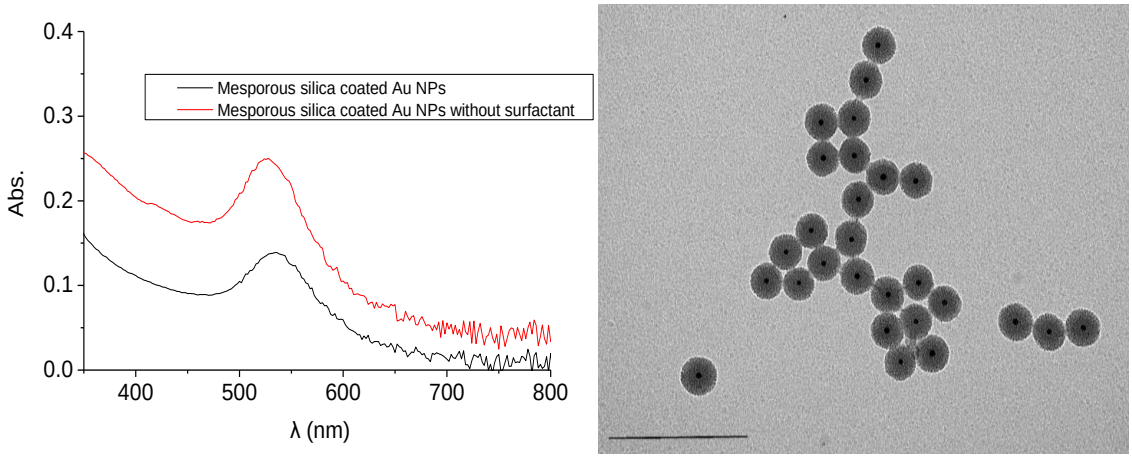

Figure 19. UV-Vis spectra of Au seeds coated with a mesoporous layer of silica (black) and after the surfactant was eliminated from the pores (red). On the right, TEM image of Mesoporous silica-coated Au NPs with CTAB in ethanol, scale bar 200 nm.

4.1.4 Step 4

Finally, in the fourth step, gold was branched through the silica pores, by adding more $HAuCl_4$ as well as HCl, $AgNO_3$ and AA.

Here $AgNO_3$ is added to stimulate the anisotropic growth of the tips of the stars, because it gives asymmetry by stabilizing defects, since gold has a close-packed, face-centered cubic structure, and being so symmetrical is difficult to form tips during the growth.

An UV-Vis spectrum done (Figure 20) confirming that Au nanostars were indeed obtained, with a very broad band as it was stated in the Introduction; it represents the plasmon band of the gold core and multiple plasmon bands corresponding to the tips and core–tip interaction. These findings align with a previous study by Steckiewicz KP et al. [10], which anticipated a range of 500-1400 nm; however, the spectrophotometer used in this case was limited to measurements up to 800 nm.

The results revealed with software *ImageJ* in Figure 20 showed that the average diameter for the silica layer is preserved, and the golden branches were satisfactorily grown, with an average length of around 15 nm.

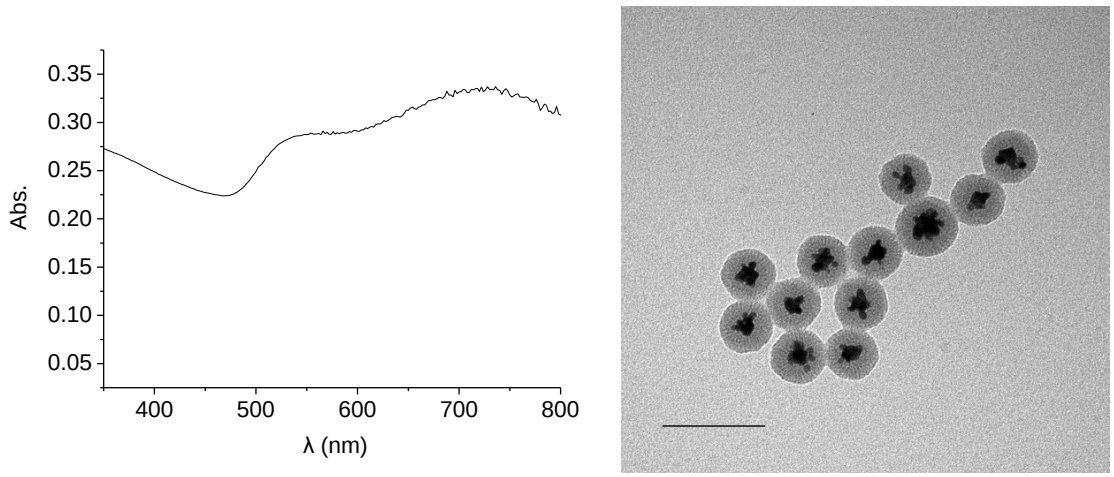

Figure 20. UV-Vis spectra of Au nanostars and its TEM image, scale bar 100 nm.

As it can be seen in Figure 21, where the UV-Vis of Au NSs and Au nanostars are compared, the shape of the NPs causes large changes in the spectra.

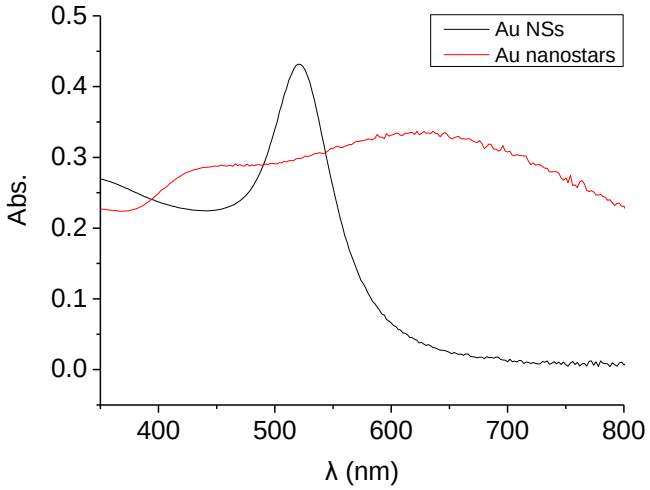

Figure 21. Comparation between the spectrum of Au NSs (black) and nanostars (red).

4.2 Synthesis chiral gold nanostars

The same experimental procedure as for the achiral gold nanostars was used for synthesizing chiral ones, adding several amounts of **CS1** and CTAB, to assess the correct proportions needed to make the particles not aggregate, but it failed. Unfortunately, in none of the experiments was it possible to go beyond the step of growing the silica layer, and none of the options yielded stable gold nanostars, despite its initially reddish appearance, none of the methods tried yielded the desired result. TEM

images were made after the growing of silica layer, and they revealed that **CS1** behaved strangely with the NPs and made them look as if they were aggregated. The growth of the silica layer did not meet the anticipated expectations, as it's shown in Figure 22, where it is evident that none of the Au nanostars underwent this growth process. This could possibly be attributed to the low affinity of the Cl^- in **CS1** for the gold surface.

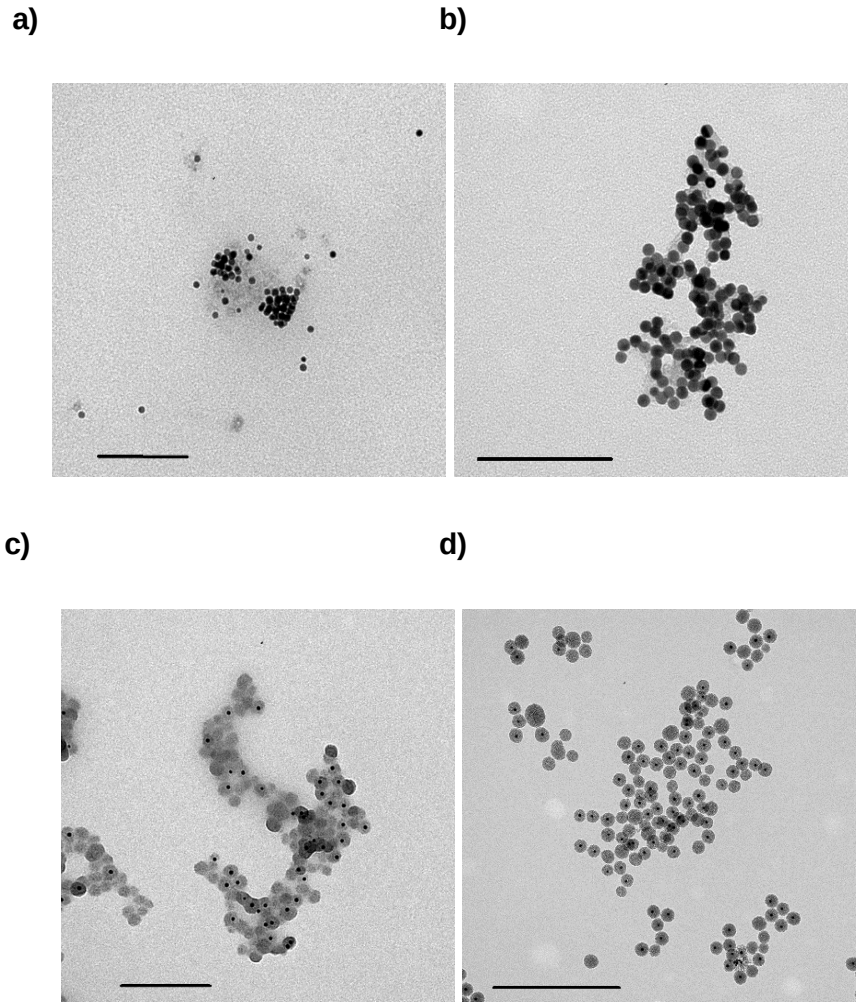

Figure 22. TEM images. **(a)** Experiment LS10 (2 mM **CS1**), scale bar 100 nm **(b)** Experiment LS11 (0.25 mM **CS1**), scale bar 100 nm **(c)** Experiment LS13 (0.1 mM **CS1**), scale bar 200 nm **(d)** Experiment LS12 (Control CTAB), scale bar 0.5 µm.

Since plenty of silica without gold nuclei inside were seen, it was thought that the silica layer did not nucleate on the gold particles and remained outside of them, so other sources of silica were tested with groups that had a greater affinity for gold owing to the presence of amino and thiol groups. Additional experiments were carried out, trying different sources of silica in addition to TEOS, incorporating APTES and Silanethiol (structures depicted in Figure 23), to enhance the growth of the silica layer.

These silica precursors bind covalently to the surface of the Au NPs via a strong Au–S bond or Au-N, and thus, it is easier for the silica layer to grow around the Au NP since it already has a silanol group attached.[36]

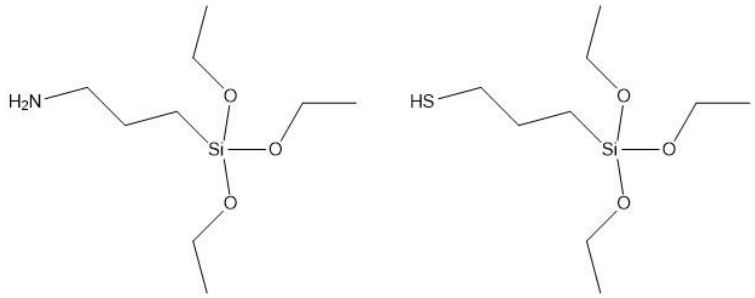

Figure 23. APTES (left) and Silanethiol structures (right).

As some solutions were blue, it could easily be seen that they were aggregated, and this was already a clue that the silica layer had not formed around them. The others that were red colored were also unable to grow the silica layer around the Au NP nuclei, but this was not known until they were taken to TEM, and images shown in Figure 24 were obtained.

a) **b)**

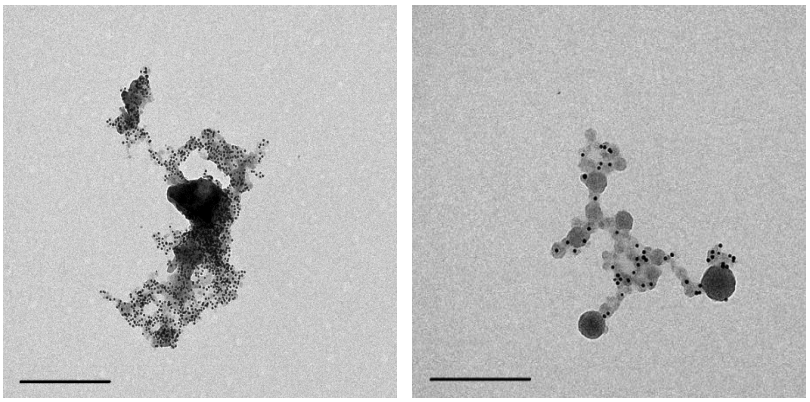

Figure 24. TEM images. **(a)** Experiment LS16, 2% Silane, scale bar 0.5 μm **(b)** Experiment LS18, 5% APTES.

The experiments with 5 % of thiol and 10% APTES were discarded before being taken to TEM because after heating in the silicone bath, before they were centrifugated, it was clearly seen that they were aggregated as they had blue color.

Chiral gold nanostars could not be achieved through the method reported by N. Sanz-Ortiz M et al.[20] with **CS1**.

4.3 Synthesis chiral surfactant

Since the silica layer did not grow around Au NPs in the experiments tested with the chiral surfactant **CS1**, a new chiral surfactant called **CS2** was synthesized to be used in future studies.

The synthesis illustrated in Figure 25 led to the formation of **CS2.**

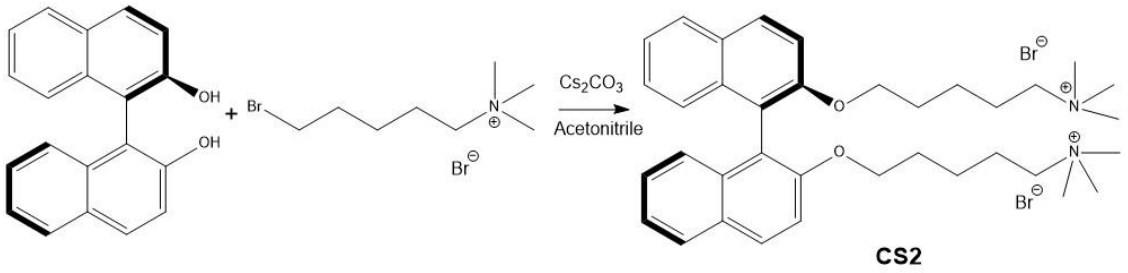

Figure 25. Synthesis of **CS2.**

The reaction that takes place is a nucleophilic substitution S_N2. In this mechanism, the nucleophilic oxygens present in the phenol groups of (R)-BINOL act as electron-rich species and attack the electrophilic carbon atom of the 5-bromo-N,N,N-trimethylpentan-1-aminium bromide. The S_N2 mechanism involves a concerted reaction, meaning that the nucleophilic attack and expulsion of the leaving group occur simultaneously. In this case, the bromine atom in 5-bromo-N,N,N-trimethylpentan-1-aminium bromide serves as a good leaving group. It has a weak bond with the carbon atom, making it susceptible to substitution by the incoming nucleophile.

(R)-BINOL exhibits axial chirality due to its molecular structure having a central axis that prevents it from being rotated to align with its mirror image. This configuration is highly stable, and its enantiomerically pure forms are commercially available. Utilizing (R)-BINOL as a building block allows the synthesis of chiral molecules, such as surfactants like **CS2,** with specific stereochemical properties.[37]

During the reaction, the nucleophilic attack by the oxygens of BINOL displaces the bromine atom, resulting in the formation of a new bond between the carbon atom and the nucleophile. This leads to the formation of **CS2**.

It is also important to note that the choice of acetonitrile as a polar aprotic solvent and cesium carbonate as a strong base provides suitable conditions for the S_N2 mechanism

to occur. The acetonitrile solvent facilitates the solvation of the reactants, while cesium carbonate enhances the nucleophilicity of the attacking species.

The synthesized product was characterized by ^{1}H-NMR spectroscopy and to achieve correct structural elucidation, ^{13}C-NMR spectroscopy and MS spectrometry were also used. MS spectrum is shown in the Appendix. For the analysis of all the spectra, the program MestReNova 6.0 of Mestrelab Research S.L. was used.

The ^{1}H-NMR spectrum in Figure 26 shows twelve signals. The reason behind this can be attributed to the surfactant´s hydrogens, which possess a closely resembling chemical environment due to the presence of a C_2 axis that induces rotational motion in the naphthalene groups, causing them to behave as if they were equivalent. It is important to note that despite lacking a plane of symmetry due to its chirality, this phenomenon still occurs. So, they appear as a single signal integrated by several hydrogens. The same happens for the ^{13}C-NMR spectrum.

There are three different groups of signals; the doublets between 1.22 – 4.48 ppm that correspond to both aliphatic chains; the signals between 7.36 – 8.37 ppm that correspond to the aromatic hydrogens, and the singlet presents at 3.31 ppm, corresponding to methyl protons of the amine groups that integrates for 18 hydrogens.

This spectrum shows that the surfactant was synthesized with both aliphatic chains.

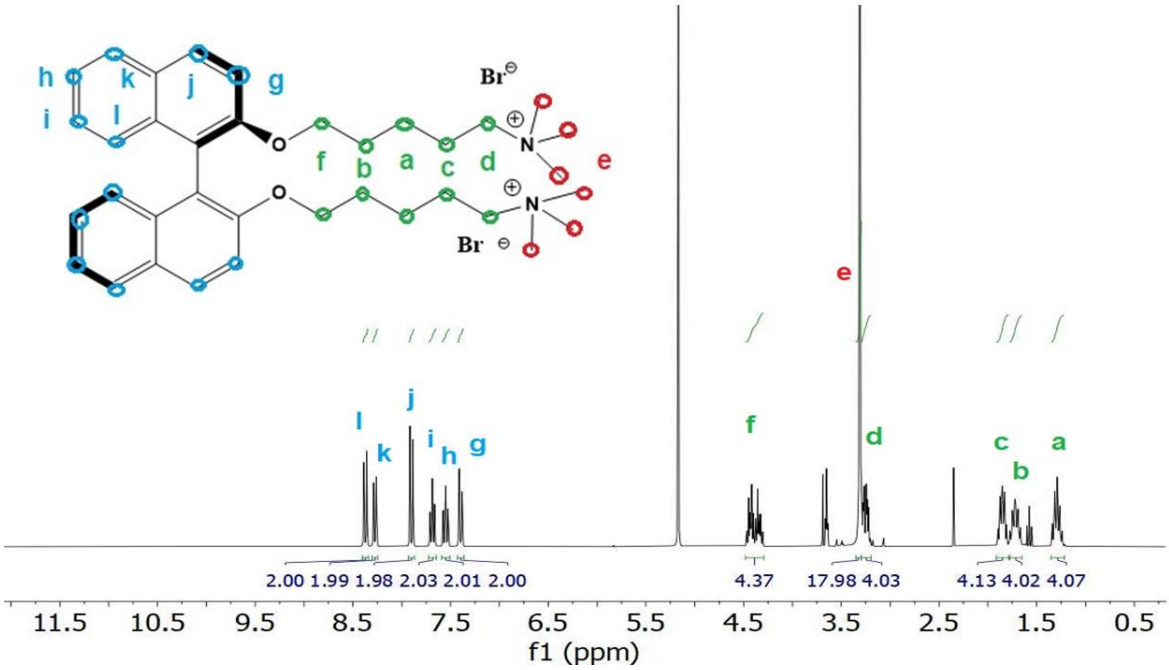

Figure 26. ^{1}H-RMN in MeOD which confirms the structure of **CS2**.

The ^{13}C-NMR spectrum in Figure 27 shows sixteen signals, the largest one at 47 ppm corresponds to the solvent used, MeOD. Here it can also be seen the three different groups of signals; the ones between 10 – 70 ppm that correspond to both aliphatic chains, the ones between 110 – 160 ppm that correspond to the aromatic carbons of the rings, and the signal present at 53.5 ppm, corresponding to methyl groups of the amine.

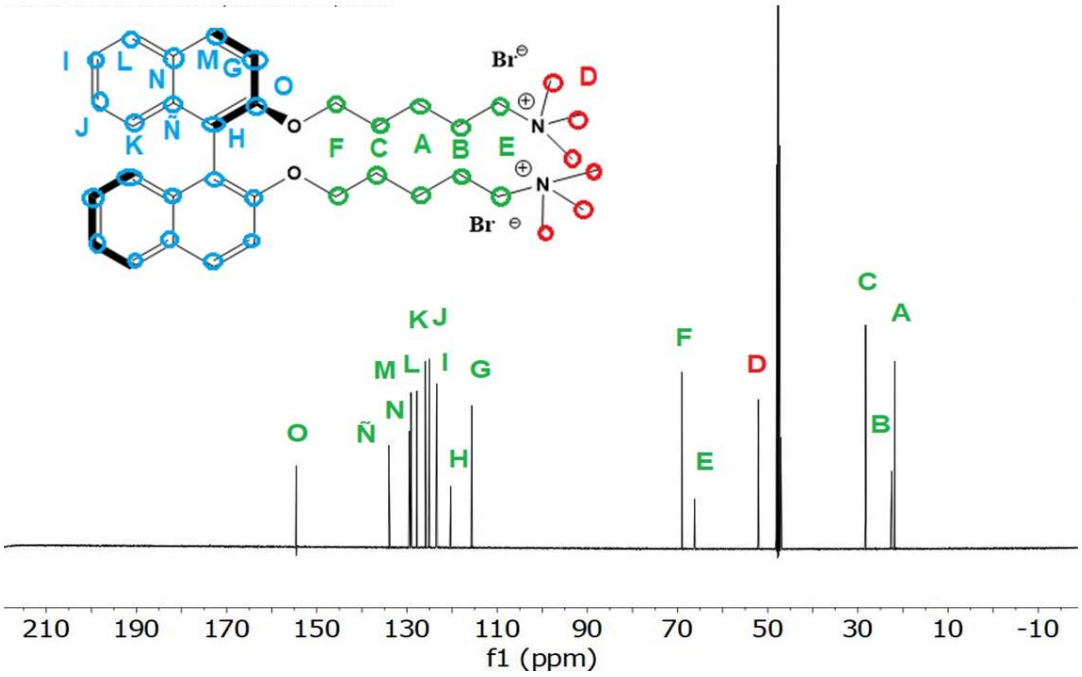

Figure 27. ^{13}C-RMN in MeOD of **CS2**.

The surfactant was also characterized by ESI$^+$-MS, which confirmed that the obtained product corresponds to the chemical formula $[C_{38}H_{54}Br_2N_2O_2]^+$ (the signal with a m/z of 271.200 belongs to the molecular ion $[C_{38}H_{54}Br_2N_2O_2]^+$).

5. Conclusions

Taking into account the proposed objectives and the results obtained in this project, the following conclusions can be drawn:

1. The synthesis of gold nanostars based on the paper reported by N. Sanz-Ortiz M et al.[20] could be replicated. Using TEM and UV-Vis, it has been showed that Au seeds, nanospheres and nanostars can be successfully synthesized and characterized by following the described procedure.

2. Chiral surfactant **CS1** was not capable of inducing a homogenous silica shell growth over the Au NSs. An additional strategy using silica precursors with higher affinity to gold was explored, but it was not improved the results.

3. A chiral surfactant was synthesized and characterized by ^{1}H-NMR and ^{13}C-NMR spectroscopy and MS spectrometry.

Even though the experimental results did not meet expectations, this study has provided valuable insight into the challenges associated with the synthesis and characterization of gold nanostars.

Conclusións

Tendo en conta os obxectivos propostos e os resultados obtidos neste proxecto, pódense extraer as seguintes conclusións:

1. A síntese de nanoestrelas de ouro a partir do artigo publicado por N. Sanz-Ortiz M et al.[20] pudo ser replicada. Usando TEM e UV-Vis, demostrouse que as sementes de Au, as nanoesferas e as nanoestrelas poden sintetizarse e caracterizarse con éxito seguindo o procedemento descrito.

2. O surfactante quiral **CS1** non foi capaz de inducir un crecemento homoxéneo da capa de sílice nas nanosferas de ouro. Explorouse unha estratexia adicional que utilizaba precursores de sílice con maior afinidade polo ouro, pero non mellorou os resultados.

3. Sintetizouse un surfactante quiral e caracterizouse mediante espectroscopia ^{1}H-RMN e ^{13}C-RMN e espectrometría MS.

A pesar de que os resultados experimentais non cumpriron as expectativas, este estudo proporcionou unha valiosa información sobre os desafíos asociados á síntese e caracterización das nanoestrelas de ouro.

Conclusiones

Teniendo en cuenta los objetivos propuestos y los resultados obtenidos en este proyecto, se pueden extraer las siguientes conclusiones:

1. La síntesis de nanoestrellas de oro basadas en el artículo publicado por N. Sanz-Ortiz M et al.[20] ha podido ser replicada. Usando TEM y UV-Vis, se ha demostrado que las semillas de Au, las nanoesferas y las nanoestrellas se pueden sintetizar y caracterizar con éxito siguiendo el procedimiento descrito.

2. El surfactante quiral **CS1** no fue capaz de inducir un crecimiento homogéneo de la capa de sílice sobre las nanoesferas de oro. Se exploró una estrategia adicional utilizando precursores de sílice con mayor afinidad por el oro, pero no mejoró los resultados.

3. Se sintetizó un surfactante quiral y se caracterizó mediante espectroscopía de ^{1}H-NMR y ^{13}C-NMR y espectrometría de MS.

A pesar de que los resultados experimentales no cumplieron con las expectativas, este estudio ha brindado información valiosa sobre los desafíos asociados con la síntesis y caracterización de las nanoestrellas de oro.

6. Appendix

a. Mass spectrum

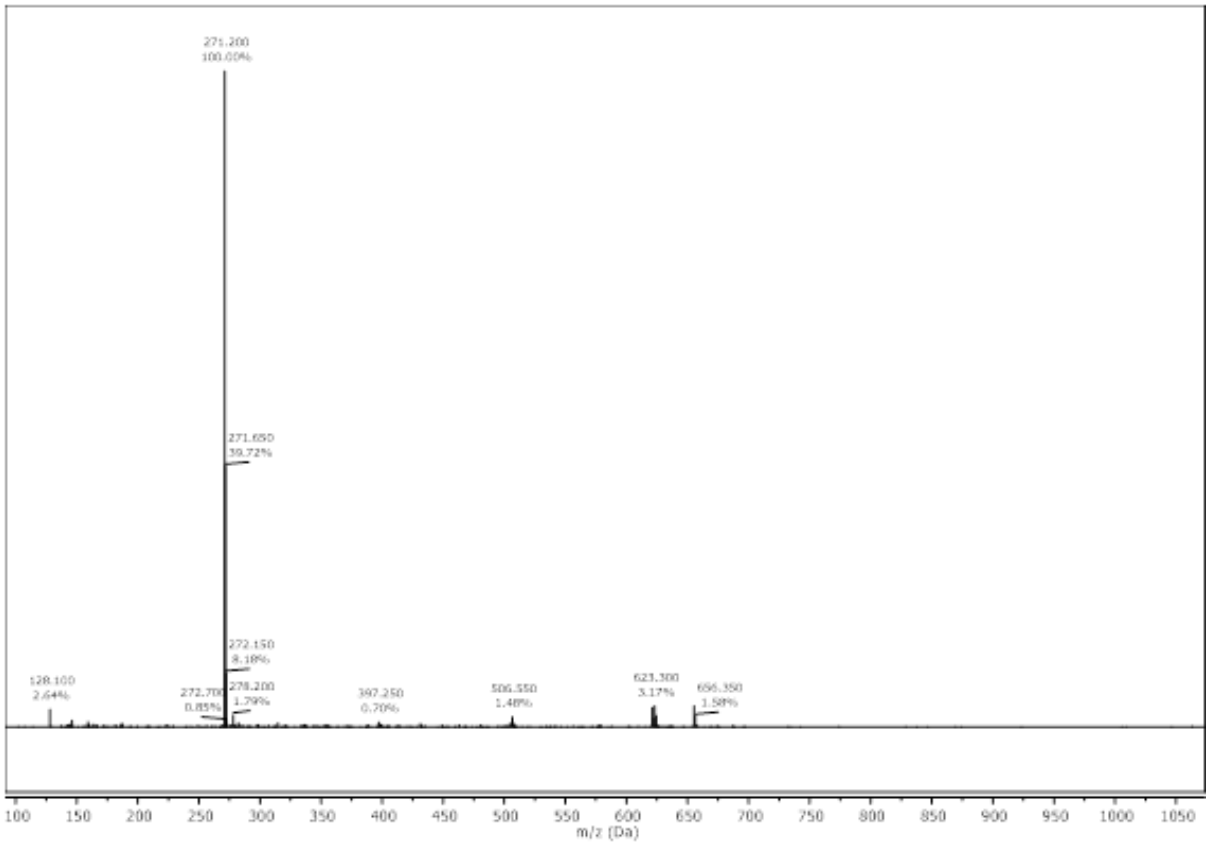

Figure X. ESI+ -MS spectrum of the synthesized chiral surfactant. calculated m/z for $[C_{38}H_{54}Br_2N_2O_2]^+$: m/z: 271.193

7. Bibliography

1. Ghosh, S. K. & Pal, T. Interparticle Coupling Effect on the Surface Plasmon Resonance of Gold Nanoparticles: From Theory to Applications. (2007) doi:10.1021/cr0680282.
2. Pitkethly, M. J. as building blocks? Nanoparticles. (2003).
3. Bayda, S., Adeel, M., Tuccinardi, T., Cordani, M. & Rizzolio, F. The History of Nanoscience and Nanotechnology: From Chemical–Physical Applications to Nanomedicine. *Molecules 2020, Vol. 25, Page 112* **25**, 112 (2019).
4. Mosquera, J. *et al.* Plasmonic Nanoparticles with Supramolecular Recognition. *Adv. Funct. Mater* **30**, 1902082 (2020).
5. Scarabelli, L. Recent advances in the rational synthesis and self-assembly of anisotropic plasmonic nanoparticles. *Pure and Applied Chemistry* **90**, 1393–1407 (2018).
6. Schlücker, S. & Schlücker, S. Spectroscopic Methods Surface-Enhanced Raman Spectroscopy: Concepts and Chemical Applications Angewandte Reviews. doi:10.1002/anie.201205748.
7. Gerber, A., Bundschuh, M., Klingelhofer, D. & Groneberg, D. A. Gold nanoparticles: Recent aspects for human toxicology. *Journal of Occupational Medicine and Toxicology* **8**, 1–6 (2013).
8. Yeh, Y.-C., Creran, B. & Rotello, V. M. Gold nanoparticles: preparation, properties, and applications in bionanotechnology. doi:10.1039/c1nr11188d.
9. Gautier, C. & Bürgi, T. Chiral Gold Nanoparticles. *Chem. Phys. Chem.* **10**, 483–492 (2009).
10. Steckiewicz, K. P. *et al.* Impact of gold nanoparticles shape on their cytotoxicity against human osteoblast and osteosarcoma in in vitro model. Evaluation of the safety of use and anti-cancer potential. *J. Mater Sci. Mater Med.* **30**, 1–15 (2019).
11. Li, N. *et al.* Anisotropic Gold Nanoparticles: Synthesis, Properties, Applications, and Toxicity. *Angewandte Chemie International Edition* **53**, 1756–1789 (2014).

12. Moreira, A. F., Rodrigues, C. F., Reis, C. A., Costa, E. C. & Correia, I. J. Gold-core silica shell nanoparticles application in imaging and therapy: A review. *Microporous and Mesoporous Materials* **270**, 168–179 (2018).

13. Kedia, A. & Kumar, P. S. Controlled reshaping and plasmon tuning mechanism of gold nanostars. *J. Mater Chem. C Mater* **1**, 4540–4549 (2013).

14. Swarnapali, A., Indrasekara, D. S., Thomas, R. & Fabris, L. Plasmonic properties of regiospecific core-satellite assemblies of gold nanostars and nanospheres †. *Phys. Chem. Chem. Phys* **17**, 21133 (2015).

15. Prabha, S., Durgalakshmi, D., Rajendran, S. & Lichtfouse, E. Plant-derived silica nanoparticles and composites for biosensors, bioimaging, drug delivery and supercapacitors: a review. doi:10.1007/s10311-020-01123-5ï.

16. Slowing, I. I., Trewyn, B. G., Giri, S. & Lin, V. S. Y. Mesoporous Silica Nanoparticles for Drug Delivery and Biosensing Applications. *Adv. Funct. Mater* **17**, 1225–1236 (2007).

17. Kankala, R. K. *et al.* Nanoarchitectured Structure and Surface Biofunctionality of Mesoporous Silica Nanoparticles. *Advanced Materials* **32**, 1907035 (2020).

18. Mehmood, A., Ghafar, H., Yaqoob, S., Gohar, U. F. & Ahmad., B. Mesoporous Silica Nanoparticles: A Review. *J. Dev. Drugs* **6**, 1–14 (2017).

19. Vazquez, N. I., Gonzalez, Z., Ferrari, B. & Castro, Y. Synthesis of mesoporous silica nanoparticles by sol–gel as nanocontainer for future drug delivery applications. *Boletín de la Sociedad Española de Cerámica y Vidrio* **56**, 139–145 (2017).

20. N. Sanz-Ortiz, M., Sentosun, K., Bals, S. & M. Liz-Marzán, L. Templated Growth of Surface Enhanced Raman Scattering-Active Branched Gold Nanoparticles within Radial Mesoporous Silica Shells. *ACS Nano* **9**, 10489–10497 (2015).

21. Zheng, G. *et al.* Discrete metal nanoparticles with plasmonic chirality. *This journal is Cite this: Chem. Soc. Rev* **50**, 3738 (2021).

22. Wu, W. & Pauly, M. Chiral plasmonic nanostructures: recent advances in their synthesis and applications. *Cite this: Mater. Adv.* **3**, 186 (2022).

23. Three causes of chirality in nanostructures. (i) The helical structure... | Download Scientific Diagram. https://www.researchgate.net/figure/Three-causes-of-chirality-in-nanostructures-i-The-helical-structure-of-a-gold_fig1_332711710.

24. Zheng, G. *et al.* Discrete metal nanoparticles with plasmonic chirality. *Chem. Soc. Rev.* **50**, 3738–3754 (2021).

25. González-Rubio, G. *et al.* Micelle-directed chiral seeded growth on anisotropic gold nanocrystals. *Science (1979)* **368**, 1472–1477 (2020).

26. Hendel, T. *et al.* In Situ Determination of Colloidal Gold Concentrations with UV−Vis Spectroscopy: Limitations and Perspectives. *Anal. Chem.* **86**, (2014).

27. Valls, A., Altava, B., Aseyev, V., García-Verdugo, E. & Luis, S. V. Imidazolium based gemini amphiphiles derived from L-valine. Structural elements and surfactant properties. *J. Mol. Liq.* **341**, 117434 (2021).

28. Gonzaíez-Rubio, G. *et al.* Disconnecting Symmetry Breaking from Seeded Growth for the Reproducible Synthesis of High Quality Gold Nanorods Article. *ACS Nano* **13**, 45 (2019).

29. Amina, S. J. & Guo, B. A Review on the Synthesis and Functionalization of Gold Nanoparticles as a Drug Delivery Vehicle. *Int. J. Nanomedicine* **Volume 15**, 9823–9857 (2020).

30. Abdullah, A. *et al.* Facile room temperature synthesis of multifunctional CTAB coated gold nanoparticles. *Chem. Phys.* **510**, 30–36 (2018).

31. Picciolini, S., Mehn, D., Ojea-Jiménez, I., Gramatica, F. & Morasso, C. Hydroquinone Based Synthesis of Gold Nanorods. *J. Vis. Exp.* **2016**, 54319 (2016).

32. He, Y. Q., Liu, S. P., Kong, L. & Liu, Z. F. A study on the sizes and concentrations of gold nanoparticles by spectra of absorption, resonance Rayleigh scattering and resonance non-linear scattering. *Spectrochim. Acta. A. Mol. Biomol. Spectrosc.* **61**, 2861–2866 (2005).

33. Hua, Z., Yu, T., Liu, D. & Xianyu, Y. Recent advances in gold nanoparticles-based biosensors for food safety detection. *Biosens. Bioelectron.* **179**, 113076 (2021).

34. Aggregation of gold nanoparticles (AuNPs) and the corresponding... | Download Scientific Diagram. https://www.researchgate.net/figure/Aggregation-of-gold-nanoparticles-AuNPs-and-the-corresponding-absorption-spectrum-a_fig1_343668822.

35. Tsyganenko, A. A. *et al.* Brønsted acidity of silica silanol groups induced by adsorption of acids. *Catal. Letters* **70**, 159–163 (2000).

36. Gao, J., Huang, X., Liu, H., Zan, F. & Ren, J. Colloidal stability of gold nanoparticles modified with thiol compounds: Bioconjugation and application in cancer cell imaging. *Langmuir* **28**, 4464–4471 (2012).

37. Krajnc, M. & Niemeyer, J. BINOL as a chiral element in mechanically interlocked molecules. *Beilstein J. Org. Chem* **2022**, 508–523 (2022).